GEOLOGY, MINERAL EQUILIBRIA, SULFUR, RUBIDIUM-STRONTIUM AND LEAD ISOTOPES AND INTRUSION CHEMISTRY OF THE McDAME TUNGSTEN SKARN PROSPECT, NORTH CENTRAL BRITISH COLUMBIA

by

BRADFORD JAMES COOKE

B.Sc., Queen's University, 1976

A THESIS SUBMITTED IN PARTIAL FULFILLMENT OF THE REQUIREMENTS FOR THE DEGREE OF MASTER OF SCIENCE

in

FACULTY OF GRADUATE STUDIES

Department of Geological Sciences

We accept this thesis as conforming to the required standard

THE UNIVERSITY OF BRITISH COLUMBIA

October, 1983

In presenting this thesis in partial fulfilment of the requirements for an advanced degree at the University of British Columbia, I agree that the Library shall make it freely available for reference and study. I further agree that permission for extensive copying of this thesis for scholarly purposes may be granted by the head of my department or by his or her representatives. It is understood that copying or publication of this thesis for financial gain shall not be allowed without my written permission.

Department of GEOLOGICAL SCIENCES

The University of British Columbia
1956 Main Mall
Vancouver, Canada
V6T 1Y3

Date NOVEMBER 18, 1983

DE-6 (3/81)

ABSTRACT

The McDame tungsten skarn prospect occurs in Hadrynian to Ordovician clastic and carbonate metasediments near Cretaceous felsic stocks. Three prograde skarn and ore facies and one retrograde facies are lithologically and structurally controlled. Prograde massive calcsilicate W-Mo-Fe facies, characterized by garnet skarn with disseminated scheelite and molybdenite, has replaced graphitic marble in contact with biotite hornfels and is thicker near a northeast striking fault. Banded calcsilicate Fe facies, typified by quartz skarn, has replaced biotite hornfels as envelopes around fractures. Banded oxide W-Mo-Fe facies, distinguished by magnetite skarn with laminations of molybdoscheelite, has replaced graphitic dolomite as veins within fractures. Retrograde massive sulfide Fe-Zn-Cu-W facies, identified by pyrrhotite skarn with disseminated sphalerite, chalcopyrite and scheelite, has replaced the other skarn facies, and locally graphitic marble, in veins and pods.

Lithostatic pressure during formation of McDame skarns was in the order of 1500 bars. Temperature and mole fraction conditions of the metasomatic fluid are estimated for the different skarn facies by assuming an idealized iron-free system. Massive garnet skarn was stable to Tmax = 555°C and Xmax = 0.14; garnet-bearing quartz skarn formed below Tmax = 475°C and Xmax = 0.08; feldspar-bearing magnetite skarn formed above Tmin = 430°C and Xmin = 0.06; and massive pyrrhotite skarn altered previously formed skarns at lower T and XCO_2. Calcsilicate mineral zoning resulted from dissolution, infiltration/diffusion and deposition of SiO_2, CaO, Al_2O_3, MgO,

H_2O and CO_2 in the skarn protoliths. Metallic mineral zoning, on the other hand, formed from W-, Mo-, O_2- and S_2-bearing magmatic fluids that reacted with country rocks to produce prograde facies, and mixed with Fe-, Zn-, and Cu-bearing formational waters to form retrograde skarn.

Sulfur isotope data from McDame porphyry, skarn and hornfels form six discrete groups (skarn average $\delta^{34}S = +7.7$) between ordinary magmatic sulfur ($\delta^{34}S = 0$) and Cambrian sedimentary sulfate ($\delta^{34}S = +30$). Their distribution can be explained by fractionation of magmatic sulfur through reaction of metasomatic fluids with wall rocks to form porphyry pyrite, skarn pyrite and skarn pyrrhotite, and mixing with formational sulfur in connate waters to produce skarn pyrrhotite-sphalerite-chalcopyrite and porphyry pyrrhotite. Rubidium-strontium isotopes from Kuhn stock quartz feldspar porphyry define a 69 ± 2 Ma isochron with a high initial ratio of 0.712, indicating that the Kuhn stock had a sialic crustal component. Isotopic disequilibrium between mineral phases suggests progressive contamination of the granitic melt by continental crust during magma ascent and crystallization. Lead isotope data from vein and skarn deposits near Cassiar cluster around the upper crustal "shale" curve for the Canadian Cordillera, indicating an upper crustal source for the lead. Thus, anatexis and assimilation of continental crust produced granitic melts rich in lithophile elements. The Kuhn stock is an oxidized granitoid of sedimentary origin, geochemically specialized in K_2O, K/Rb, U and U/Th and anomalous in W and Mo. Differentiation processes have concentrated these lithophile elements in

magmatic fluids that produced the McDame tungsten skarn deposit.

TABLE OF CONTENTS

LIST OF TABLES

LIST OF FIGURES

ACKNOWLEDGEMENTS

First and foremost, I would like to thank Dr. Colin Godwin for his inspiration and guidance in supervising my thesis. From field and lab work to text writing and editing, Colin's input has been invaluable. The manuscript has also benefitted from critical reviews by Drs. A.J. Sinclair, H.J. Greenwood, T.H. Brown and R.L. Armstrong.

My thanks go to Shell Canada Resources Ltd. and, in particular, Dr. A.B. Baldwin and G. Moffat for funding the field work and providing chemical analyses and thin sections of the rocks. The British Columbia Ministry of Energy, Mines and Petroleum Resources is gratefully acknowledged for a financial grant towards thesis research and I thank Dr. A. Panteleyev for his fruitful discussions on geology near Cassiar.

Many people at U.B.C. contributed to my thesis but I wish to acknowledge Krista Scott for potassium, rubidium and strontium isotope analyses; Bruce Ryan for lead isotope analyses; Joe Harakal for argon isotope analyses; Ernie Perkins for computer programs and expertise; John Newlands for drafting and photography; and Ed Montgomery for generally being helpful.

Last but not least, I thank my wonderful wife, Susan Banks Cooke, for her moral and financial support throughout the past three years. Her patience and understanding made my work more rewarding and the thesis a success.

INTRODUCTION

Cassiar, in north-central British Columbia, has been an important mining district since 1873 when placer gold was discovered in Troutline Creek (Fig. 1). Cassiar Asbestos Mine was not developed until the early 1950's, but more recently the Cassiar area has undergone a rennaissance in mineral exploration for W, Sn, Mo, U, and Au. The McDame tungsten skarn prospect, six kilometres north of Cassiar, was discovered in 1978 by the late Bill Kuhn who panned scheelite from stream sediments. There are two zones of economic interest: 1) the A zone, which includes the Kuhn tungsten-molybdenum skarn showing, and to the west, 2) the B zone, which hosts the Dead Goat tungsten skarn and Contact silver-lead vein occurrences (Fig. 1). Detailed geologic, mineral equilibria, fluid inclusion, and sulfur, lead and rubidium-strontium isotope studies were undertaken on A zone skarns in an attempt to understand the genesis of skarn and ore minerals.

REGIONAL GEOLOGY

Cassiar lies within the Omenica Crystalline Belt (Fig. 1), one of two major regional metamorphic-plutonic belts in the Canadian Cordillera (Monger et al., 1982). Geology in the Cassiar area has been mapped on a regional scale by Gabrielse (1963) and Panteleyev (1979; 1980). Three major lithotectonic elements have been identified (Fig. 1): 1) the Cassiar platform, a miogeoclinal continental terrace wedge developed along the western margin of the North American craton in late Proterozoic to early Paleozoic times (Monger and Price, 1979), 2) the

FIG. 1. Geology of the Cassiar area (from Panteleyev, 1979; 1980), showing major lithotectonic units and Pb isotope sample sites (solid triangles). McDame prospect location and regional geological belts (ISB = Insular Belt, CPC = Coast Plutonic complex, IMB = Intermontane Belt, OCB = Omenica Crystalline Belt, RMB = Rocky Mountain Belt) are inset lower left. McDame mineral occurrences and geological units (IG = Ingenika Group, AG = Atan Group, KG = Kechika Group, CS = Contact stock, KS = Kuhn stock) are inset upper right.

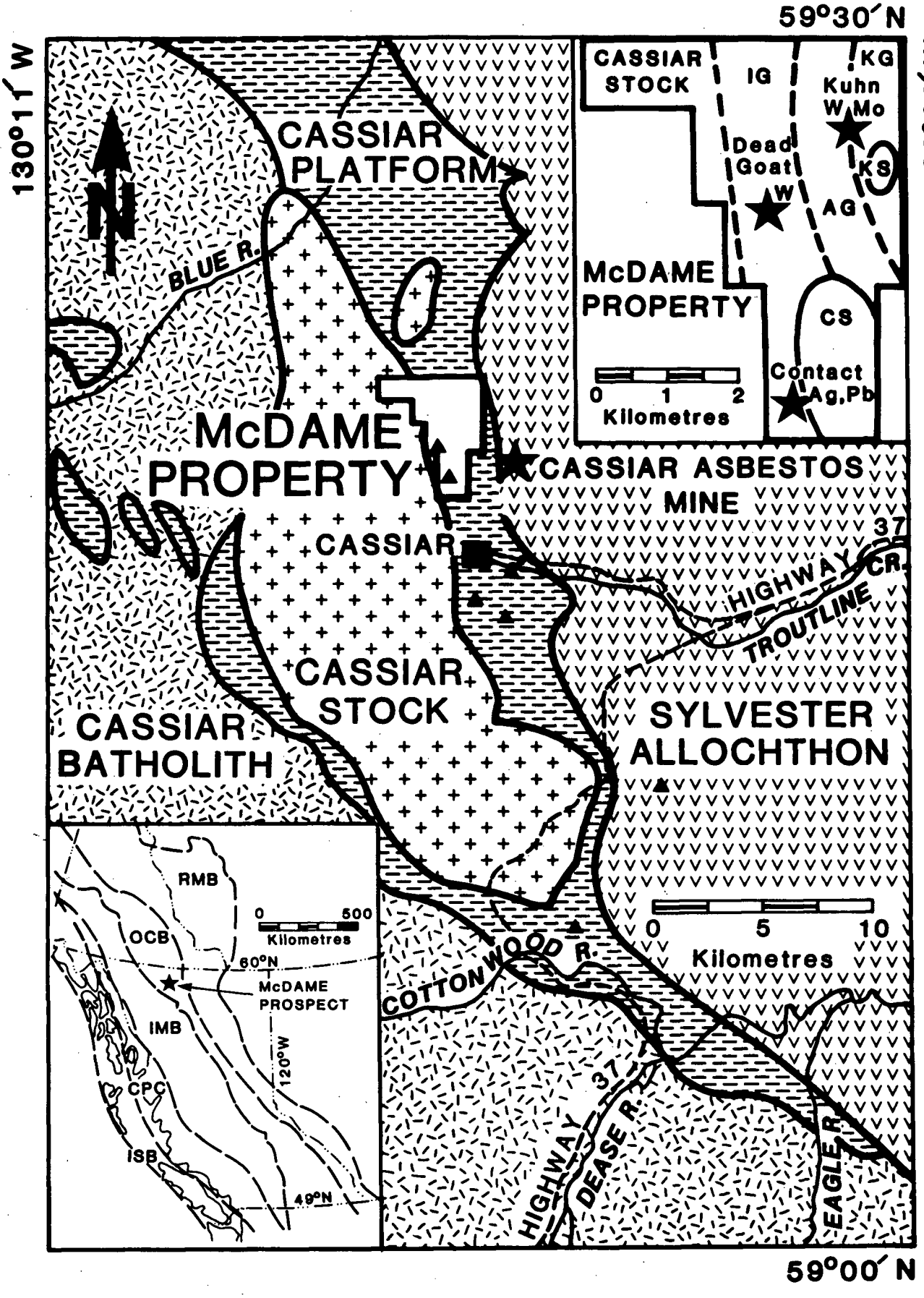
59°30′N
130°11′W
129°30′W
59°00′N
N
CASSIAR PLATFORM
BLUE R.
McDAME PROPERTY
CASSIAR
CASSIAR STOCK
CASSIAR BATHOLITH
CASSIAR ASBESTOS MINE
HIGHWAY 37
CR.
TROUTLINE
SYLVESTER ALLOCHTHON
COTTONWOOD R.
HIGHWAY 37
DEASE R.
EAGLE R.
0 5 10
Kilometres
CASSIAR STOCK
IG
KG
Kuhn W Mo
Dead Goat W
KS
AG
McDAME PROPERTY
CS
Contact Ag,Pb
0 1 2
Kilometres
RMB
OCB
IMB
CPC
ISB
0 500
Kilometres
60°N
McDAME PROSPECT
120°W
49°N

Sylvester allochthon, a late Paleozoic oceanic basin assemblage obducted onto the continental margin in middle Mesozoic times (Monger et al., 1972), and 3) the Cassiar complex, a composite plutonic belt probably related to late Mesozoic anatexis of continental crust (Tempelman-Kluit, 1979). Volcanic rocks of the Sylvester allochthon now occupy the core of the northwest trending McDame synclinorium, flanked to the west by Cassiar platformal sediments into which are intruded the Cassiar batholith and related stocks (Fig. 1).

LOCAL GEOLOGY

McDame property rocks have been subdivided into six main geological units (Table 1). Cassiar platform strata include Lower Hadrynian to Lower Ordovician metasediments of the Ingenika, Atan and Kechika Groups (units 1 to 3 respectively), crosscut by Mesozoic mafic dikes (unit 4) and Upper Cretaceous felsic stocks (unit 5). Skarn (unit 6) replaces marble, dolomite and hornfels up to several hundred meters away from the nearest felsic intrusion. Units 1 to 3 form the steeply east-dipping western limb of the McDame synclinorium. Only minor folding is apparent on the property and the associated foliation, lineation, and joint directions correspond respectively with the axial plane, fold axis, and a-c plane of the McDame synclinorium (Cooke and Godwin, 1982). One fault, with an apparent left-hand strike slip of about 120 m, was mapped in the A zone (Fig. 2).

Ingenika Group

Ingenika Group rocks underlie the B zone and contain the

TABLE 1. Correlation of Geological Units Near Cassiar

Tectonic Element Age and Group	Gabrielse 1963	Panteleyev 1980	Mansy 1979	Fritz 1980	This Paper
					Unit_6i skarn
Metasomatic Contact					
Cassiar Complex Late Cretaceous Cassiar batholith Cassiar stock Contact stock Kuhn stock Windy stock	quartz monzonite granodiorite granite porphyry aplite pegmatite	porphyritic biotite quartz monzonite: Unit_8i coarse grained Unit_8i mantled feldspar Unit_Gi quartz feldspar porphyry Unit_Qi medium grained			Unit_5i a) biotite quartz monzonite b) quartz feldspar porphyry c) aplite-pegmatite sills
Intrusive Contact					
Middle Mesozoic					Unit_4i biotite lamprophyre dikes
Intrusive Contact					
Sylvester Allochthon Devonian to Permian Sylvester Group	greenstones sediments	Unit_Gi diorite greenstones			
Fault Contact					
Cassiar Platform Cambrian to Ordovician Kechika Group	Upper? black shale black slate minor limestone Lower? limestone phyllite minor conglomerate (Upper and Lower 320 to 820 m)	shale slate		siltstone shale	Unit_3i a) graphitic marble b) white marble g) graphitic marble h) biotite hornfels (520 m)
Conformable Contact					
Cassiar Platform Lower Cambrian Atan Group	Upper? limestone dolomite minor shale	Upper? dolomite marble limestone minor slate	quartzite siltstone shale limestone	Rosella Formation limestone minor dolomite minor shale basal sandstone (695 m)	Unit_2i a) graphitic marble b) grey marble c) white marble d) graphitic dolomite e) grey dolomite f) white dolomite (140 m)
	Lower? quartzite argillite slate shale siltstone conglomerate (980 m Upper and Lower)	Lower? hornfels argillite quartzite		Boya Formation quartzite siltstone shale (400 m)	g) graphitic hornfels h) biotite hornfels i) cordierite hornfels j) muscovite hornfels k) quartz hornfels (380 m)
Conformable Contact					
Cassiar Platform Hadrynian-Cambrian Ingenika Group	Good Hope Group limestone dolomite quartzite sandstone siltstone argillite shale slate limestone (1310 m)	Good Hope Group Upper? marble limestone Lower? hornfels quartzite phyllite schist skarn	Stellus Formation shale siltstone sandstone (273 m) limestone dolostone (125 m) redbed limestone dolostone slate (86 m) slate minor limestone (529 m)	siltstone minor quartzite minor shale	Unit_1i i) cordierite hornfels (400 m) marble dolomite (100 m) hornfels marble skarn (200 m)

FIG. 2. Geology of the A zone, showing distribution of the main rock and skarn types (1i = Ingenika Group cordierite hornfels; 2a,d,h,i,k = Atan Group graphitic marble, graphitic dolomite, biotite hornfels, cordierite hornfels, quartz hornfels; 3g,h = Kechika Group graphitic hornfels, biotite hornfels; 4a = biotite lamprophyre dikes; 5a = Contact stock biotite quartz monzonite, 5b = Kuhn stock quartz feldspar porphyry; 6a = massive calcsilicate skarn, 6g = banded calcsilicate skarn, 6h = banded oxide skarn) and the location of S isotope (solid triangles) and Rb-Sr isotope (solid square) samples.

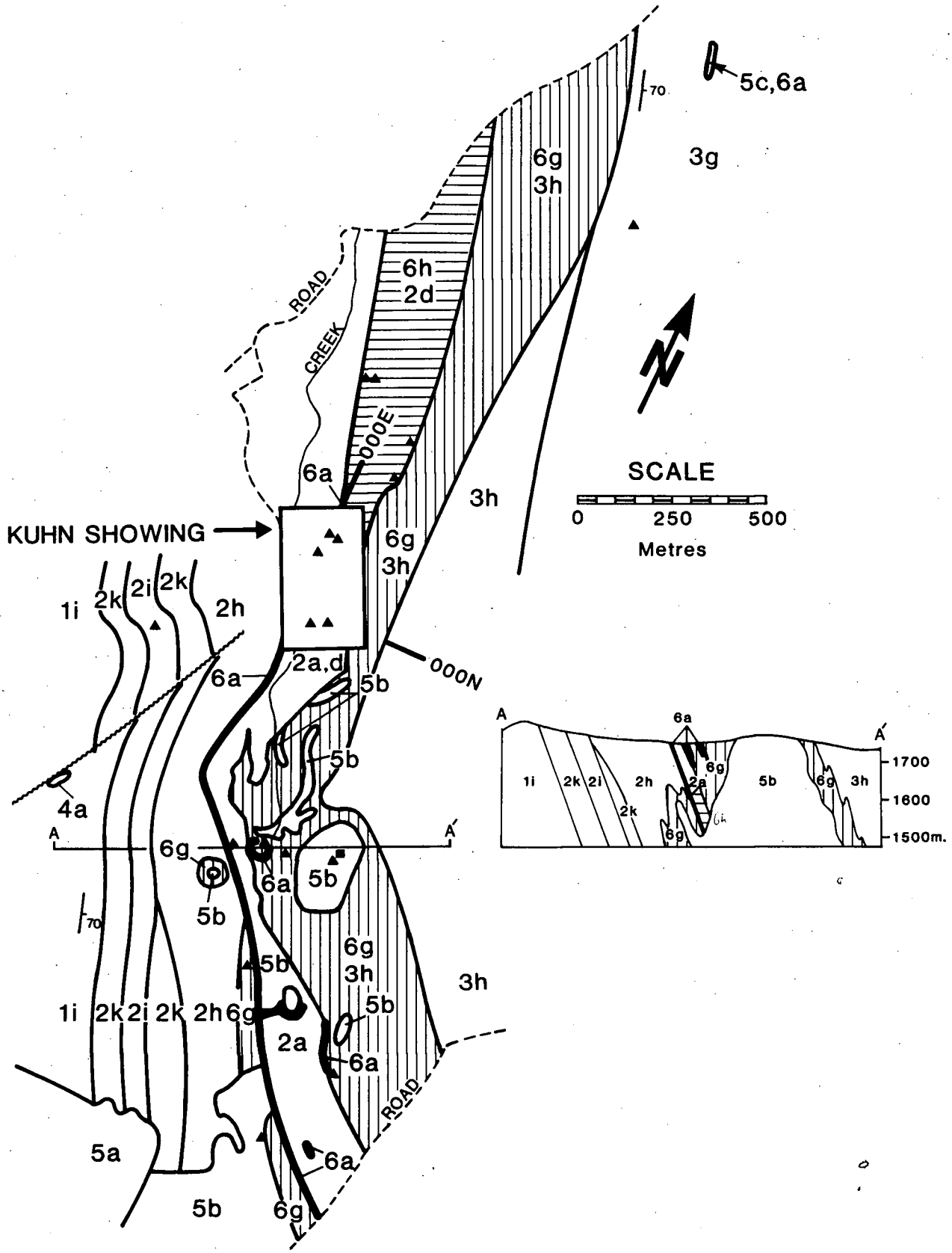

Cooke and Godwin

Dead Goat and Contact showings (Fig. 1). Ingenika Group rocks represent the westernmost exposures of stratified rocks on the McDame property and form three metasedimentary bands (Figs. 1 and 2). From west to east, these are:

1) interbanded biotite hornfels, white marble and bimetasomatic garnet-pyroxene skarn, in contact with the Cassiar stock to the west,

2) banded graphitic and massive grey marbles, with minor graphitic dolomite lenses, containing rare zebra textured patches (stromatolites?) up to several meters thick and concentrically banded pods (stromatoporoids?) up to 20 cm across, and

3) spotted cordierite hornfels (Fig. 2: unit 1i), with minor biotite and muscovite hornfels and rare white marble bands. These three rock bands correlate respectively with the redbed (interbedded limestone, dolostone and slate), carbonate and clastic layers in the upper part of the Stelkuz Formation mapped by Mansy (Mansy and Gabrielse, 1978; Mansy, 1979) east of the McDame synclinorium (Table 1).

Atan Group

Atan Group rocks underlie the western part of the A zone and include the Kuhn showing. The strata are conformable with the Ingenika Group and consist of two metasedimentary bands (Fig. 2). From west to east, these are:

1) banded biotite hornfels (unit 2h), with layers of spotted cordierite and massive quartz hornfels (units 2i, 2k) and partings of foliated muscovite hornfels (unit 2j),

2) banded graphitic marble (unit 2a), with layers of massive grey and white marbles (units 2b, 2c) south of the Kuhn showing that interfinger towards the north into zebra textured graphitic dolomite (unit 2d), interlayered with massive grey and white dolomite (units 2e, 2f). Rare dolomite breccias contain concentrically banded lenses and nodular pods with ovoid horns up to 5 cm long (archeocyathids?). These two metasedimentary bands are lithologically similar to clastic and carbonate sedimentary rocks of the Boya and Rosella Formations respectively as mapped by Fritz (1978; 1980) elsewhere in north-central British Columbia (Table 1).

Kechika Group

Kechika Group rocks underlie the eastern part of the A zone (Fig. 2). They are conformable with the Atan Group and consist of thinly interbanded hornfels, including banded graphitic and biotite hornfels (units 3g, 3h), with minor layers of banded graphitic and massive white marbles (units 3a, 3c). These rocks are comparable to interbedded clastic and carbonate rocks of the Kechika Group as mapped by Gabrielse (1963) and Panteleyev (1979; 1980) near Cassiar (Table 1).

Mafic Intrusions

Biotite lamprophyre dikes intrude older stratified rocks, but are themselves crosscut by younger skarn veins. The dikes appear to have been emplaced along pre-skarn faults (Fig. 2) and are probably Mesozoic in age (Table 1).

Felsic Intrusions

Felsic intrusions comprise the Cassiar batholith and four discrete stocks on the McDame property (Fig. 2). Biotite quartz monzonite (unit 5a) is typical of the Cassiar and Contact stocks whereas quartz feldspar porphyry (unit 5b) characterizes the Kuhn and Windy stocks. Minor aplite and pegmatite sills (unit 5c) intrude both sedimentary and plutonic rocks (Table 1).

SKARN AND ORE FACIES

Skarns on the McDame property can be classified into four metasomatic facies (Table 2). The massive calcsilicate (MCF) W-Mo-Fe, banded calcsilicate (BCF) Fe and banded oxide (BOF) W-Mo-Fe facies are time equivalent prograde skarns that formed in different rock types. Massive sulfide (MSF) W-Cu and Zn-W zones are retrograde skarns that replaced the other skarn facies. Calcsilicate mineral zoning is typical of prograde skarn and metallic mineral zoning characterizes retrograde skarn.

Massive Calcsilicate Facies

Massive calcsilicate skarn (MCF) occurs as semi-continuous bands up to 10 m thick along the western or lower contacts of the marble bands in the Ingenika and Atan Groups, as smaller lenses at their eastern or upper contacts, and as small pods within the marbles themselves (Figs. 3, 4). At the Kuhn showing, massive garnet skarn (unit 6a) passes easterly through massive pyroxene skarn (unit 6b) into dolomite, and westerly through massive epidote skarn (unit 6c) into hornfels. In the A zone, massive amphibole skarn (unit 6d) comprises small pods in

TABLE 2: Mineral Assemblages and Abundances in Dolomite, Marble, Hornfels and Skarn

MINERAL ASSEMBLAGES		garnet GA	pyroxene PX	epidote EP	amphibole AM	plagioclase PL	scapolite SC	corundum CO	chlorite CL	talc TA	biotite BI	muscovite MU	orthoclase OR	spheene SP	tourmaline TO	apatite AP	zircon ZI	garnet GR	dolomite DO	calcite CA	quartz QZ	fluorite FL	scheelite SH	molybdoscheelite MS	molybdenite MO	chalcopyrite CP	sphalerite SL	stibnite SB	pyrrhotite PR	pyrite PY	magnetite MG	hematite HE
SKARN																																
Massive Calcsilicate Facies	MCF																															
garnet skarn	GS	5	3	L	1	L			1	L	L			L		L				2	2	L	C	R	C	R		R	C	L	R	
pyroxene skarn	PS	L	5	L	2				1		L			L		L				2	2	1	L			R	L	R	C			
epidote skarn	ES	L	L	5	2				2					2		1				1	4		C						L			
amphibole skarn	AS				5				L	L										4									R			
biotite skarn	BS			3		1			1		4			L		1	L			L	5	L	L	C		L			2	1	2	
scapolite skarn	SS						5													2	2											
Banded Calcsilicate Facies	BCF																															
garnet zone	GZ	5	5	3	5				1											L	5		R	R		R			C	C		
epidote zone	EZ			5										L							5											
pyroxene zone	PZ		5	1	5	3			1					1		L					5											
amphibole zone	AZ			1	5	3	L							1		L					5											
Banded Oxide Facies	BOF																															
feldspar zone	FZ		4			3			1	1										1	L			C		R			1	2	3	R
calcite zone	CZ		3																	5											R	R
talc zone	TZ		L			L			4	4						L				4	L		R	C	R	C		R	3	1	1	R
Massive Sulfide Facies	MSF																															
pyrrhotite skarn	YS	4	3	1	1				1	L											4	2	C			C	1		4	L		
sphalerite skarn	HS	L	4																		4	1	C			L	4	R	1	L		
KECHIKA GROUP																																
Biotite Hornfels	BH			L		2			L		3			1	L	1	L				5								L	R		
ATAN GROUP																																
Graphitic Marble	GM								L									1		5									R			
Graphitic Dolomite	GD								L									1	5										R			

1. Assemblages and abundances estimated from thin and polished sections.
2. Quantitative code for abundance is: 5 = 50% to 100%, 4 = 10% to 50%, 3 = 5% to 10%, 2 = 1% to 5%, 1 = 0% to 1%.
   Qualitative code for abundance is: C = common, L = low or occasional, R = rare.

FIG. 3. Geological plan of the Kuhn showing, located in Figure 2, indicating the lensoidal nature of massive calcsilicate facies garnet skarn (6a) that has replaced Rosella Formation graphitic marble (2a, b). At trench A-2, massive calcsilicate skarn is zoned from banded biotite hornfels (2h), through 2 m of massive epidote skarn (6c), 8 m of massive garnet skarn (6a), and 20 cm of massive pyroxene skarn (6b), to zebra textured graphitic dolomite (2d). Other geological symbols are defined in Table 1.

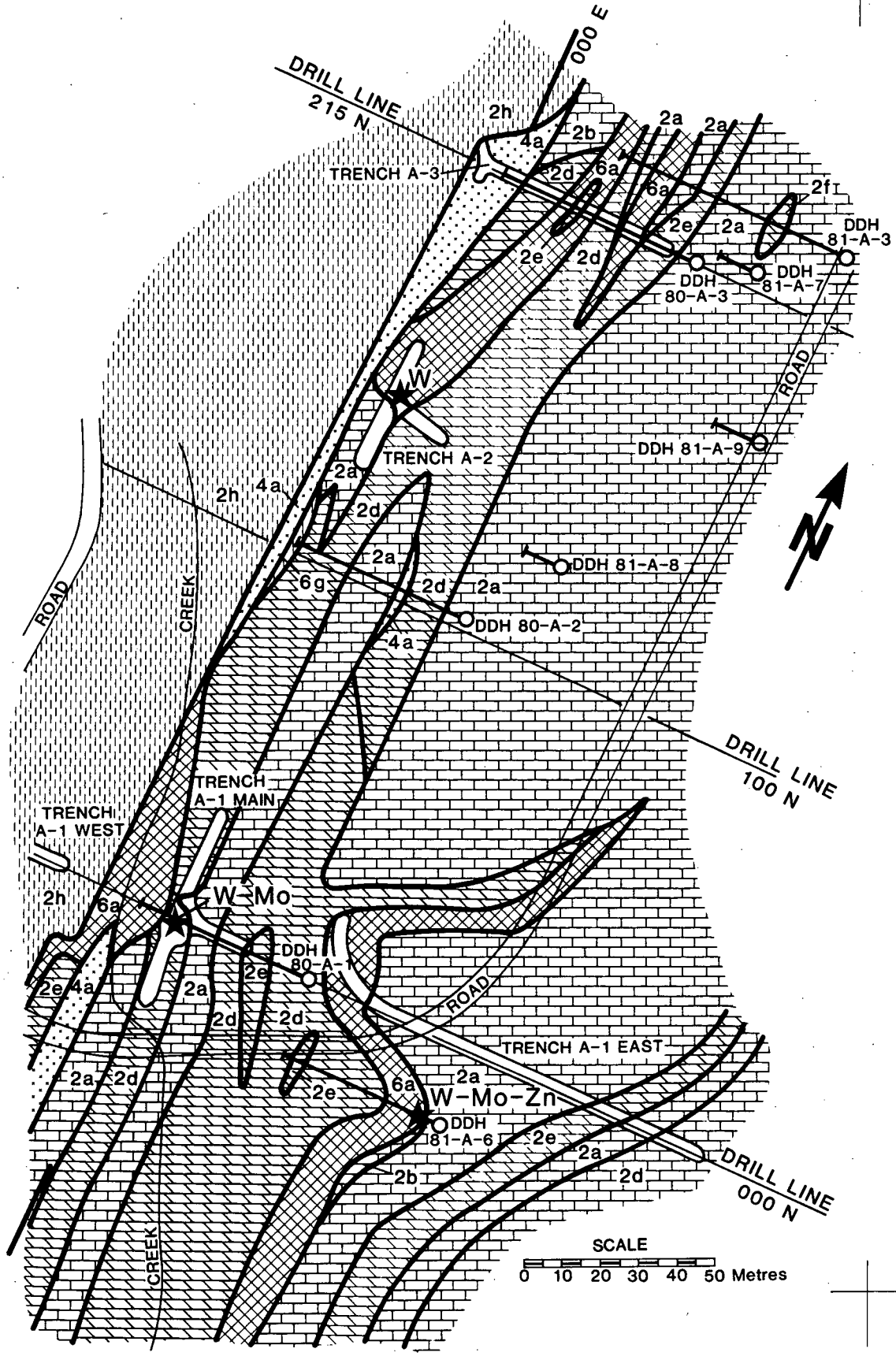

Fig. 3: Cooke and Godwin

FIG. 4. Geological section of the Kuhn showing, located in Figure 2, indicating the development of banded calcsilicate facies quartz skarn that replaced Boya Formation bleached biotite hornfels (2h), and banded oxide facies magnetite skarn that replaced Rosella Formation bleached graphitic dolomite (2f). The banded calcsilicate and banded oxide facies are both fracture controlled. Other geological symbols are defined in Table 1.

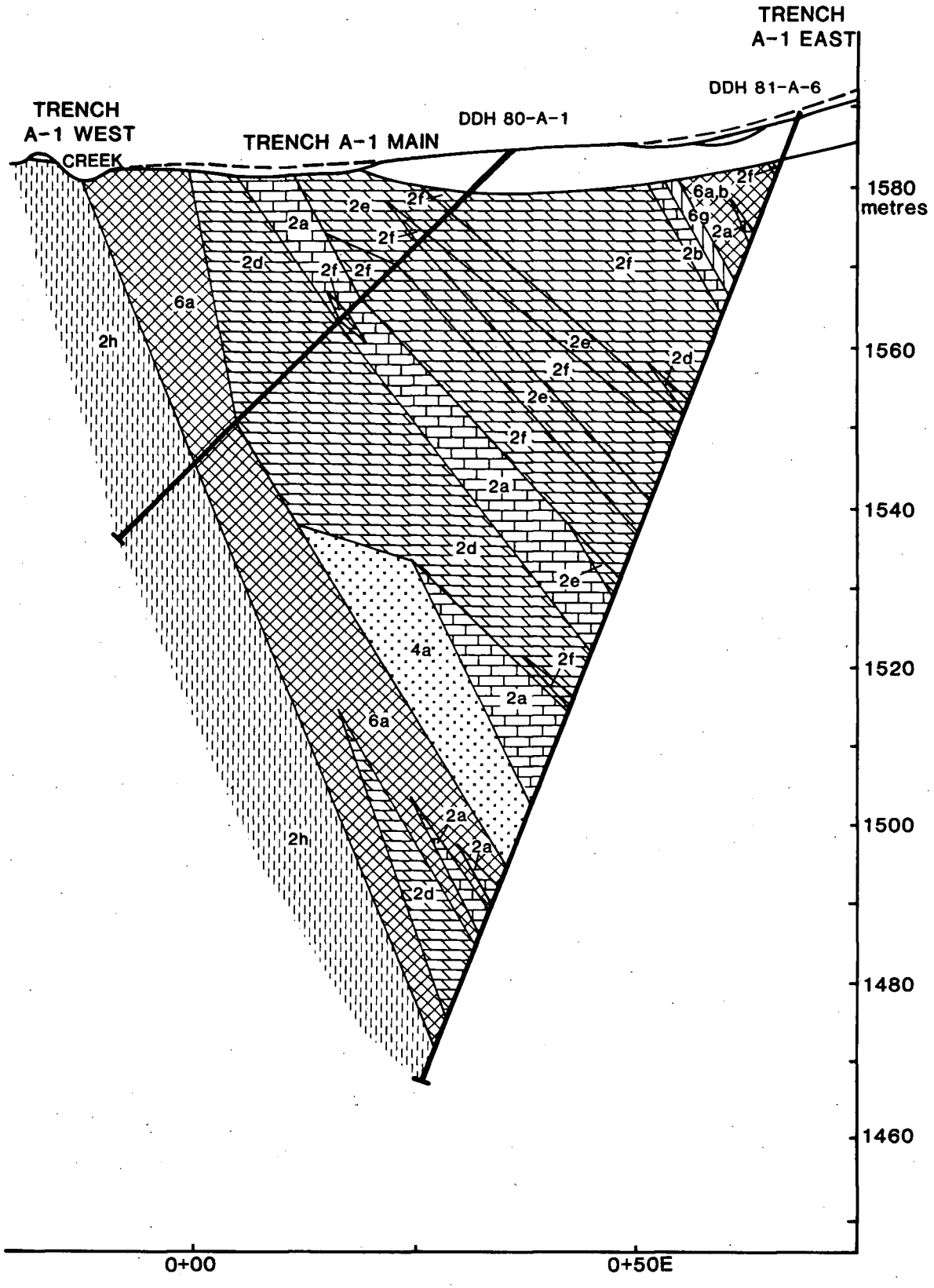

DRILL LINE 0+00 N

Fig. 4: Cooke and Godwin

dolomite adjacent to quartz feldspar porphyry dikes. Spotted biotite skarn (unit 6e) occurs within hornfels where marble and skarn are absent at the overlying dolomite contact, north of the Kuhn showing. Rare scapolite skarn (unit 6f) is found as thin layers and coarse disseminations in Kechika Group hornfels and metasomatized mafic dikes near the Kuhn showing. Scheelite (occasionally rimmed by molybdoscheelite), molybdenite, pyrite, pyrrhotite and rare magnetite form coarse disseminations interstitial to calcsilicates at the Kuhn showing. Tungsten and molybdenum grades are higher near the core of the massive calcsilicate facies whereas trace contents of copper and zinc (associated with pyrrhotite and pyrite) increase at the skarn contacts, particularly in pyroxene skarn at its upper contact with carbonate.

Banded Calcsilicate Facies

Banded calcsilicate skarn (BCF) constitutes a bleached, quartz-rich zone up to 200 m thick within hornfels of the Kechika Group, surrounding and overlying quartz feldspar porphyry of the Kuhn stock (Figs. 1 and 2). Banded quartz skarn (unit 6g) occurs as narrow, concentrically zoned, quartz-rich envelopes containing garnet, epidote, pyroxene, and amphibole around bedding plane and a-c joint fractures. Where fracture density is high, the original rock can be bleached throughout; near the Kuhn stock, quartz skarn forms a distinct alteration halo in brecciated Kechika Group rocks. Two smaller quartz skarn zones occur in Atan Group hornfels next to quartz feldspar porphyry dikes. Minor finely disseminated pyrrhotite and pyrite

occur in quartz skarns. At the Kuhn showing, quartz-molybdenite veins crosscut Atan hornfels in drill core where quartz skarn is absent.

Banded Oxide Facies

Banded oxide skarn (BOF) is composed of crisscrossing veins in zones up to tens of meters wide within Atan Group dolomites (Figs. 3, 4), locally bordering massive calcsilicate skarn north of the Kuhn showing. Banded magnetite skarn (unit 6h) forms rhythmically banded magnetite veins up to 1 m wide containing pyroxene- and plagioclase-bearing zones. Talc skarn (unit 6i) has replaced magnetite skarn near massive sulfide veins and constitutes narrow fracture fillings up to 1 cm wide south of the Kuhn showing. Molybdoscheelite, magnetite, pyrite and rare hematite form fine disseminations and laminations in banded oxide skarn. High tungsten and molybdenum grades are associated with high fluorite content in the veins. Minor amounts of copper and zinc (associated with pyrite and pyrrhotite) occur at the skarn contacts. At the Kuhn showing, stibnite and sphalerite veins crosscut Atan dolomite where magnetite skarn is absent.

Massive Sulfide Facies

Massive sulfide skarn (MSF) consists of pods and veins up to 1 m wide replacing other skarn facies, especially massive calcsilicate skarn. Massive pyrrhotite skarn (unit 6j) has replaced garnet and magnetite skarns at the Kuhn Showing but grades southwards into more sphalerite-rich skarn (unit 6k) that has replaced pyroxene skarn. Scheelite, chalcopyrite and rare

pyrite form fine disseminations in both pyrrhotite and sphalerite skarns. Tungsten and copper grades are higher in the former and zinc grades higher in the latter.

MINERAL EQUILIBRIA

Pressure, temperature and mole fraction of the skarn-forming fluids can be estimated from mineral equilibria on P-T (Fig. 5) and T-XCO_2 (Fig. 6) diagrams calculated by computer from thermodynamic data (Helgeson et al., 1978) for an iron-free, six component system (SiO_2, Al_2O_3, MgO, CaO, CO_2 and H_2O). Qualitative studies of skarn in thin section using petrographic and SEM-EDS microscopes indicate that garnet, epidote, pyroxene, amphibole and biotite at McDame contain iron. Because the stability fields of iron-bearing phases (e.g. garnet, pyroxene) in these diagrams expand at the expense of iron-free phases (e.g. wollastonite, anorthite) and minerals with lower partition coefficients for iron (e.g. epidote, amphibole, biotite), the resulting estimates of Pmax, Tmax and Xmax from the iron-free system are lower than the actual maximum conditions of formation for iron-bearing rocks at McDame.

Massive Calcsilicate Facies

The massive calcsilicate facies (MCF) is characterized by garnet skarn with the mineral assemblage garnet + pyroxene + calcite + quartz ± amphibole ± chlorite (Table 2). Grossularite-rich garnet (GS) and quartz (QZ), in the absence of wollastonite (WO) and anorthite (AN), limit the stability of garnet skarn in P-T space (Fig. 5) by the reaction:

FIG. 5. Partial P-T diagram for the system SiO_2-Al_2O_3-MgO-CaO-CO_2-H_2O, showing the intersections of two fluid-absent reactions: (1) GS + QZ = 2WO + AN, and (2) CZ = ZO, with a Tmax isochore from fluid inclusion data (Table 3) on fluorite in massive garnet skarn; mineral symbols are defined in Table 2 and text. Garnet skarn is stable to Pmax = 2600 bars and Tmax = 605°C, and where epidote is present, to Pmax = 1700 bars and Tmax = 505°C. The coexistence of garnet and epidote in the massive and banded calcsilicate facies limits lithostatic pressure during formation of McDame skarns to about 1500 bars in an iron-free system. Higher pressures occur in an iron-bearing system.

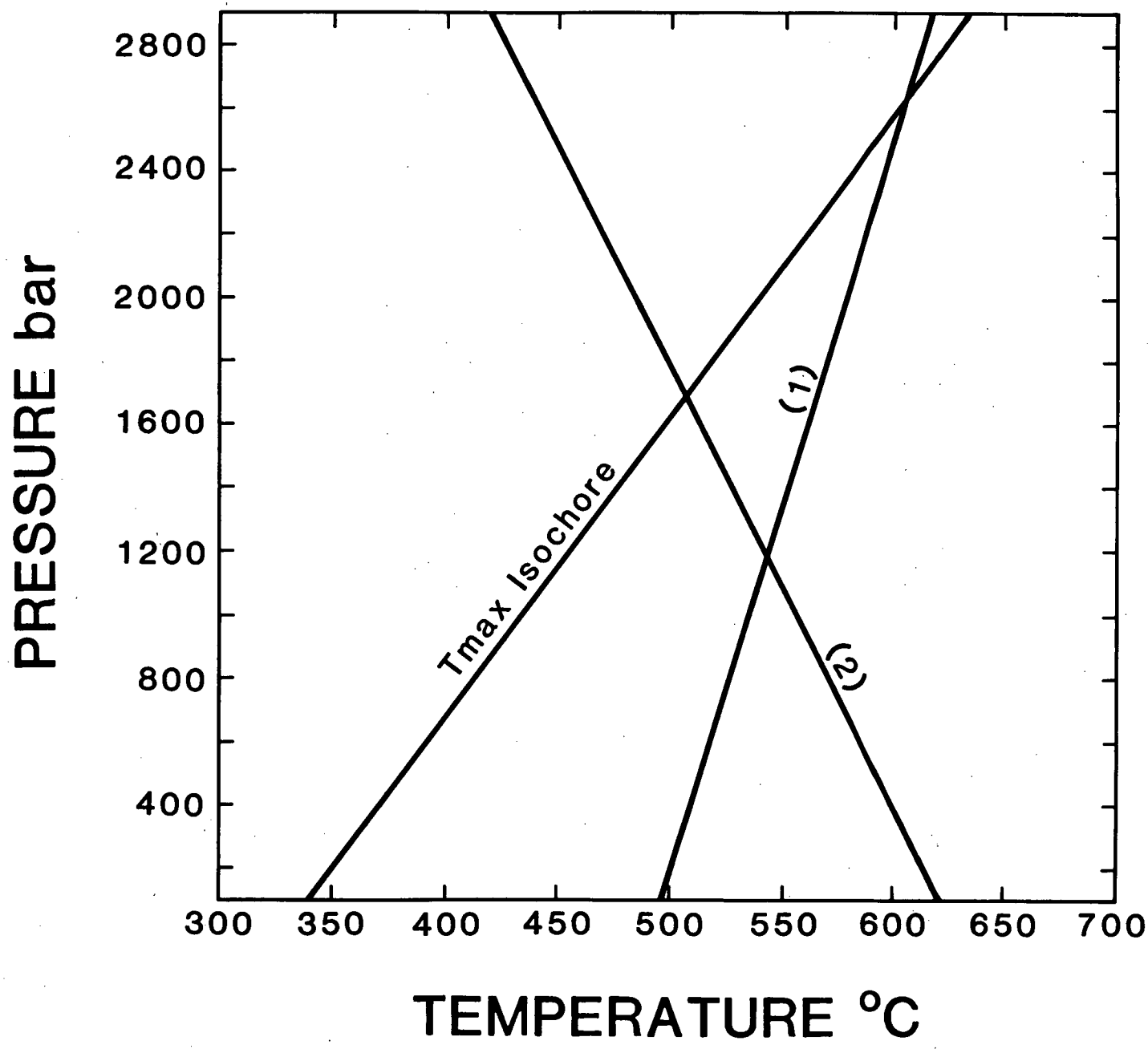

Fig.5: Cooke and Godwin

FIG. 6. Partial T-XCO_2 diagram at 1500 bars for the system SiO_2-Al_2O_3-MgO-CaO-CO_2-H_2O, showing selected skarn mineral equilibria (symbols are defined in Table 2): (1) GS + QZ = 2WO + AN, (2) CZ = ZO, (3) QZ + CA = WO + CO_2, (4) AN + QZ + 2CA = GS + $2CO_2$, (5) 2CZ + 3QZ + 5CA = 3GS + H_2O + $5CO_2$, (6) 2CZ + CO_2 = 3AN + CA + H_2O, (7) 4CZ + QZ = GS + 5AN + $2H_2O$, (8) 6CZ + TR + 2QZ = 5DI + 9AN + $4H_2O$, (9) TR + 2QZ + 3CA = 5DI + H_2O + $3CO_2$, (10) 5PH + 6CA + 24QZ = 5OR + 3TR + $2H_2O$ + $6CO_2$, (11) 3DO + 4QZ + H_2O = TA + 3CA + $3CO_2$, (12) AN + WO + CA = GS + CO_2: a) In the massive calc silicate facies (MCF), garnet skarn (crosshatched) is stable to Tmax = 555°C and Xmax = 0.14, and zoned epidote (crosses), garnet, and pyroxene (coarse stipple) skarns coexist below Tmax = 475°C and Xmax = 0.09; b) In the banded calcsilicate facies (BCF), quartz skarn (fine stipple) containing a central garnet zone has maximum T and X conditions similar to zoned massive calcsilicate skarn but is stable to lower T and X where pyroxene occupies the central zone by reaction (9) and amphibole forms from destruction of biotite (fine stipple) by reaction (10); and c) In the banded oxide facies (BOF), magnetite skarn (horizontal lines) is stable to Tmin = 430°C at Xmin = 0.06, but talc skarn (intermediate stipple) forms at lower temperatures and mole fraction CO_2 by reaction (11).

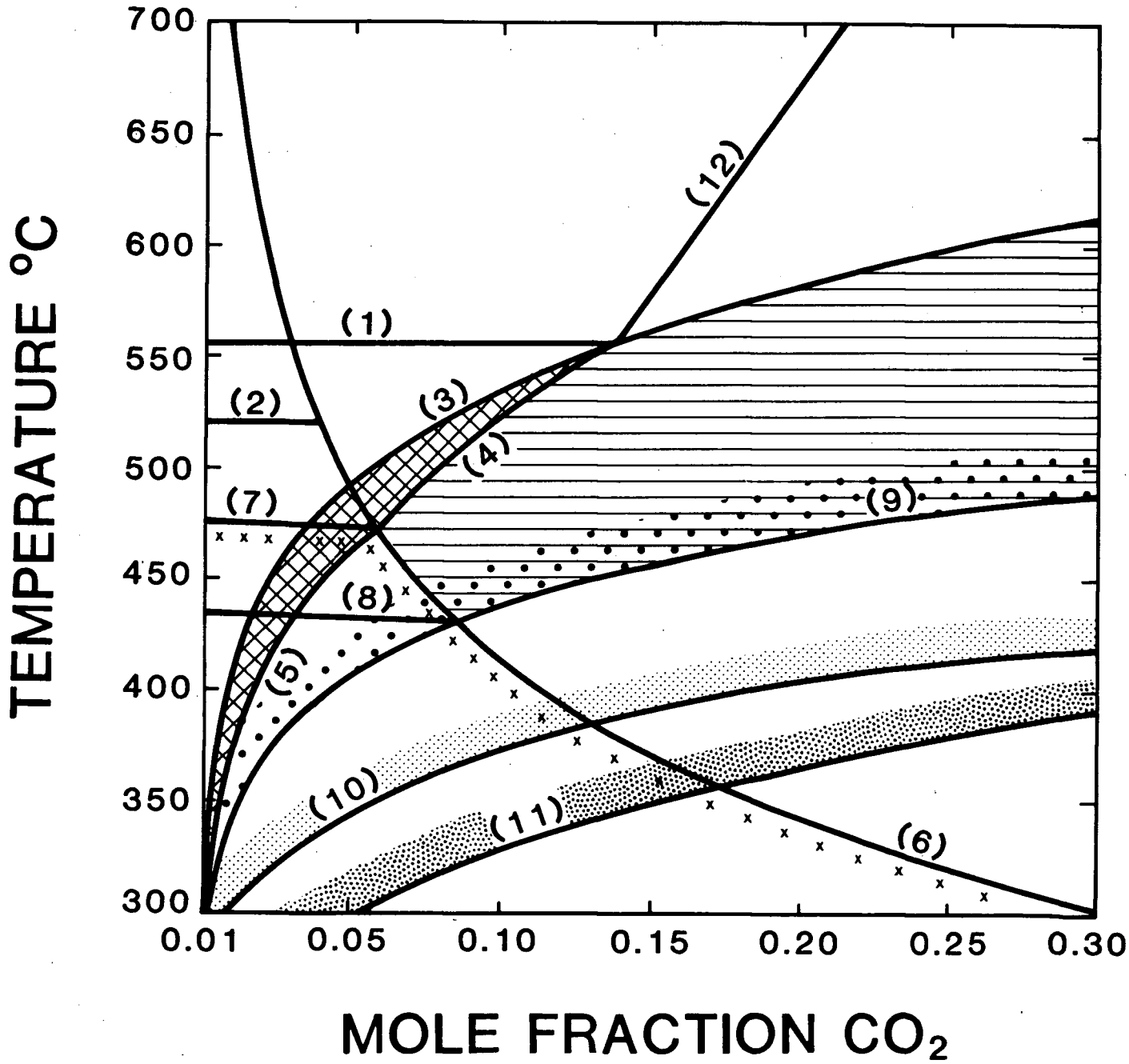

Fig. 6: Cooke and Godwin

(1) GS + QZ = 2WO + AN

Rare epidote is clinozoisite-rich (CZ) rather than zoisite-rich (ZO), limiting its stability (Fig. 5) by the reaction:

(2) CZ = ZO

Because reactions (1) and (2) are fluid-absent, their phase boundaries are not affected by the mole fractions of CO_2 and H_2O. Their intersection defines a maximum temperature for epidote-bearing garnet skarn at 545 °C (Fig. 5).

Fluid inclusion studies on rare fluorite in garnet skarn (Table 3) indicate that the skarn-forming fluid contained approximately 7% $CaCl_2$ at a maximum homogenization temperature of 350°C. Since the freezing point depression of a $CaCl_2$ fluid is similar to that of a NaCl fluid (Crawford, 1981), a constant volume and maximum temperature isochore can be plotted in P-T space (Roedder and Bodnar, 1980). The intersection of reaction (1) with the Tmax isochore (Fig. 5) locates the uppermost stability limit of garnet skarn at Pmax = 2600 bars and Tmax = 605 °C, assuming that Pfluid = Ptotal. Where epidote is present, the intersection of reaction (2) with the Tmax isochore (Fig. 5) puts the upper stability limit of garnet skarn at Pmax = 1700 bars and Tmax = 505 °C (Fig. 5). Therefore, we assume that lithostatic pressure during formation of McDame skarns is in the order of 1500 bars.

Although garnet skarn is common in the A zone (Fig. 7a), laterally zoned epidote (ES), garnet (GS) and pyroxene (PS) skarns replace graphitic marble (GM) between biotite hornfels (BH) and graphitic dolomite (GD) at the Kuhn showing (Fig. 3). Garnet skarn is restricted in T-XCO_2 space to Tmax = 555 °C and

TABLE 3. Fluid Inclusion Data from Fluorite in Garnet Skarn

Total No Inclusions	Type	Phases	V Total (cc)	V Vapor (%)	V Solid (%)	T First Melt (C)	Solid Composition	T Last Melt (C)	Density (Wt% Salt)	T Homogenization (C)
8	Primary	L+V+2S	<3x10	<5	<10	-34.5 (2)	CaCl or MgCl	-3.3 (2)	6.5	272.0 (2)
22	Primary	L+V+S	<1x10	<5	<20	-49.0 (2)	CaCl	-3.9 (3)	7.5	334.4 (2)
8	Primary	L+V	<1x10	<5	-	-	-	-	-	234.7 (1)
2	Secondary	L+V+2S	<3x10	<0.1	<5	-21.0	NaCl	-7.8	12.5	-
15	Secondary	L+V+S	<1x10	<1	<5	-21.0 (15)	NaCl	-6.3 (5)	10.0	127.0 (3)
27	Secondary	L+V	<3x10	<2	-	-21.0 (27)	NaCl	-5.8 (16)	9.3	-

1. Calculated temperatures are based on the most reliable data (number of inclusions are in parentheses) as many inclusions leaked during runs due to fractures from weathering.

FIG. 7. Modes of occurrence and mineral zoning of the four skarn facies, showing lithologic and fracture controls on skarn formation: a) massive calcsilicate facies (MCF): garnet skarn (GS) has replaced graphitic marble (GM) between Boya Formation biotite hornfels (BH) and Rosella Formation graphitic dolomite (GD); b) banded calcsilicate facies (BCF): quartz skarn (QS) includes garnet (GZ), epidote (EZ), pyroxene (PZ) and amphibole (AZ) zones enveloping fractures in Kechika and Atan Group biotite hornfels (BH); c) banded oxide facies (BOF): magnetite skarn (MG) comprises feldspar (FZ) and calcite (CZ) zones forming veins in Rosella Formation bleached graphitic dolomite (GD); and d) massive sulphide facies (MSF): pyrrhotite skarn (YS) has replaced garnet skarn and graphitic marble in pods and veins.

(a)

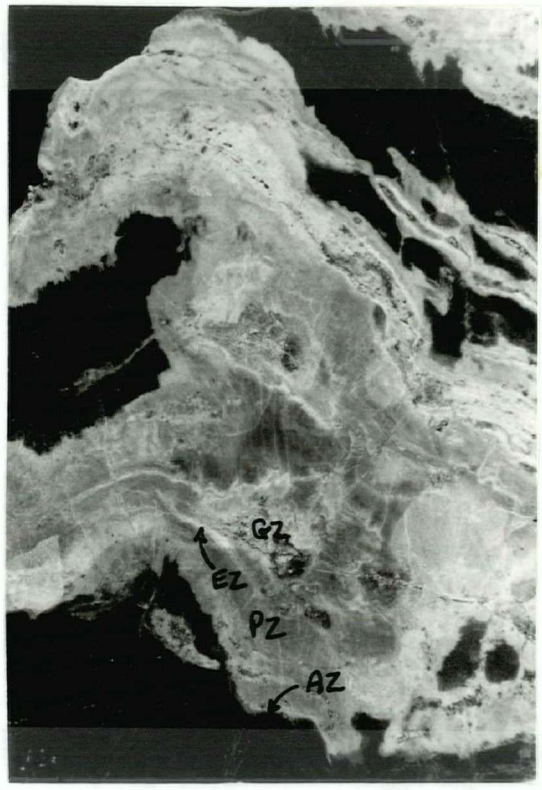

(b)

(c)

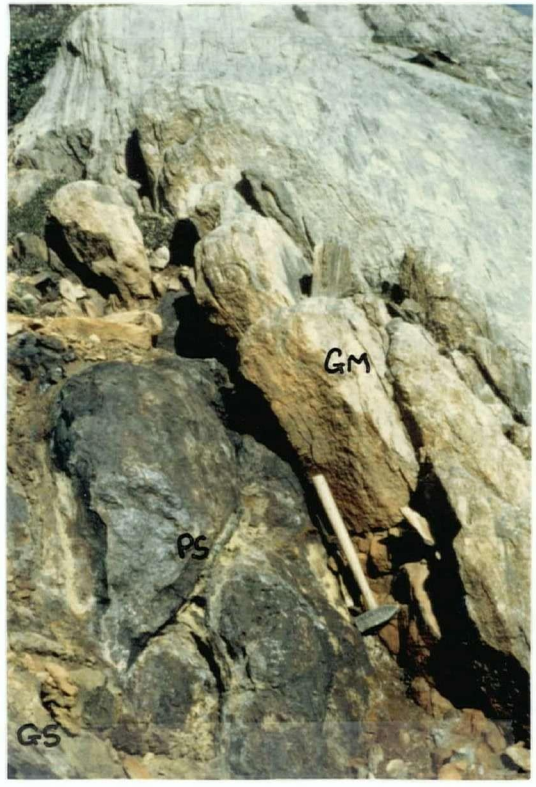

(d)

Xmax = 0.14 at P = 1500 bars by reactions involving calcite (CA) and quartz (Fig. 6):

(3) $QZ + CA = WO + CO_2$

(4) $AN + QZ + 2CA = GS + 2CO_2$

(5) $2CZ + 3QZ + 5CA = 3GS + H_2O + 5CO_2$

Epidote skarn forms below 475 °C and, where amphibole is present, below 435 °C by the reactions (Fig. 6):

(6) $2CZ + CO_2 = 3AN + CA + H_2O$

(7) $4CZ + QZ = GS + 5AN + 2H_2O$

(8) $6CZ + 2QZ + TR = 9AN + 5DI + 4H_2O$

Diopside-rich (DI) pyroxene and tremolite-rich (TR) amphibole skarns are stable under wider T-X conditions than garnet skarn by the reaction (Fig. 6):

(9) $TR + 2QZ + 3CA = 5DI + H_2O + 3CO_2$

Amphibole, calcite and quartz commonly replace pyroxene, suggesting that univariant equilibrium governed this retrograde alteration.

Mineral zoning which results dominantly from composition, pressure and temperature gradients in a flowing aqueous solution is typical of infiltrational metasomatism (Korzhinskii, 1970). Diffusion metasomatism, on the other hand, forms mineral zones in response to chemical activity gradients in a stationary pore fluid. In the A zone, Si- and Ca-bearing skarn fluids infiltrated marble in contact with hornfels to form garnet skarn. At the Kuhn showing, however, channelling of the fluids between hornfels and dolomite steepened the activity gradients of SiO_2 and CaO causing diffusion across the contacts to produce zoned garnet, epidote and pyroxene skarns. On an ACS ternary

phase diagram (Fig. 8a), a path from hornfels through skarn to dolomite is one of major increase in CaO and major decrease in SiO_2. A minor drop in Al_2O_3 also occurs at low but relatively constant MgO (buffered by dolomite and hornfels) and increasing XCO_2 (Fig. 6).

Banded Calcsilicate Facies

The banded calcsilicate facies (BCF) is typified by quartz skarn with the mineral assemblage quartz ± amphibole ± epidote ± pyroxene ± garnet ± plagioclase ± chlorite ± sphene (Table 2). Within 10 m of the Kuhn stock, quartz skarn is zoned concentrically inwards from unaltered biotite hornfels (BH) through amphibole (AZ), pyroxene (PZ) and epidote (EZ) zones to a central garnet (GZ) zone (Fig. 7b). The absence of wollastonite and anorthite, and the clinozoisite-rich composition of epidote, restrict the stability of this assemblage to P-T and T-X conditions similar to those defined for the massive calcsilicate facies. More distant from the Kuhn stock, the garnet and epidote zones are absent, pyroxene forms the central zone, and it occurs in the amphibole zone instead of epidote. This pyroxene-bearing assemblage is stable to lower T and higher XCO_2 conditions than the garnet-bearing zone (Fig. 6). Assuming that biotite is phlogopite-rich (PH) and the orthoclase (OR) component stays in solution, the destruction of biotite in hornfels occurs at even lower temperatures (Fig. 6) by the reaction:

(10) $5PH + 6CA + 24QZ = 5OR + 3TR + 2H_2O + 6CO_2$

On an ACM diagram (Fig. 8b), a path from unaltered biotite

FIG. 8. Ternary composition diagrams for the four skarn facies, showing the variation in concentration of chemical components for different mineral assemblages defined in Table 2. a) massive calcsilicate facies (MCF): biotite hornfels (BH) through zoned epidote (ES), garnet (GS) and pyroxene (PS) skarns to graphitic dolomite (GD) is a path of major increase in CaO and major decrease in SiO_2, accompanied by a minor drop in Al_2O_3 at relatively constant MgO and increasing XCO_2 (Fig. 6); b) banded calcsilicate facies (BCF): unaltered biotite hornfels (BH) through amphibole (AZ), pyroxene (PZ) and epidote (EZ) zones to a central garnet (GZ) zone is a path of major increase in CaO coinciding with minor decreases in Al_2O_3 and MgO at relatively constant SiO_2 and low XCO_2 (Fig. 6); c) banded oxide facies (BOF): bleached graphitic dolomite (GD) through a calcite (CZ) zone to a central feldspar (FZ) zone is a path of major increase in SiO_2 with a minor drop in MgO and rise in Al_2O_3 at relatively constant CaO but variable XCO_2 (Fig. 6); talc skarn (TS) replaces magnetite skarn (MS) at lower SiO_2, CaO, Al_2O_3 and XCO_2 but higher MgO; and d) massive sulfide facies (MSF): prograde skarns vary in O_2 suggesting protolith control, but their replacement by retrograde massive sulfide facies (MS) is one of major decrease in S_2. (A = Al_2O_3, C = CaO, M = MgO, S = SiO_2, f = Fe, o = O_2, s = S_2.)

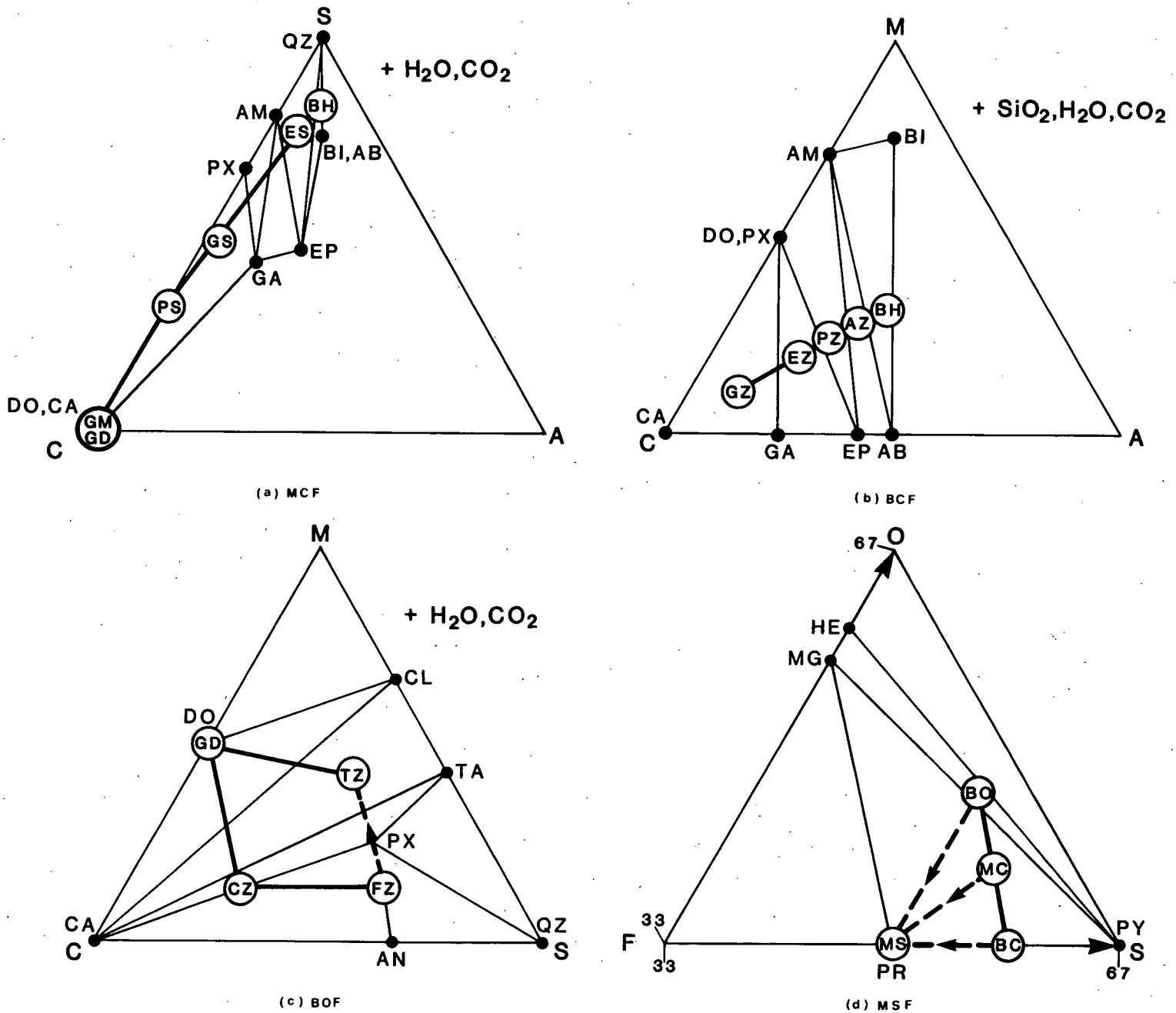

Fig. 8. Cooke and Godwin

hornfels through zoned skarn to the central garnet zone is one of major increase in CaO (calcite occurs rarely in the garnet zone). Minor decreases in Al_2O_3 and MgO occur at relatively constant SiO_2 (quartz is present in all zones) and low XCO_2 (Fig. 6). Temperatures decrease away from the Kuhn stock causing lower grade pyroxene metasomatism. However, the primary control on formation of the banded calcsilicate facies was the infiltration of Ca- and Si-bearing fluids along fractures in hornfels.

Banded Oxide Facies

The banded oxide facies (BOF) normally consists of magnetite skarn with the mineral assemblage magnetite + calcite ± pyroxene ± plagioclase ± talc ± chlorite (Table 2). North of the Kuhn showing, magnetite skarn is zoned concentrically from bleached graphitic dolomite (GD) through a pyroxene (XZ) zone to a central feldspar (FZ) zone (Fig. 7c). The absence of wollastonite, garnet, epidote and amphibole limit its stability to Tmin = 430 °C and Xmin = 0.06 (Fig. 6). Talc and chlorite, common alteration minerals of magnetite skarn, also form minor talc skarn veins in dolomite south of the Kuhn showing. This mineral assemblage is stable to lower temperatures than the pyroxene-bearing zone (Fig. 6) by the destruction of dolomite:

(11) $3DO + 4QZ + H_2O = TA + 3CA + 3CO_2$

On an SCM diagram (Fig. 8c), a path from graphitic dolomite through zoned skarn to the central feldspar zone is one of major increase in SiO_2 (quartz occurs rarely in the feldspar zone). A minor decrease in MgO and rise in Al_2O_3 occur at relatively

constant CaO (calcite is present in all zones) but variable XCO_2 (Fig. 6). Lower temperatures south of the Kuhn showing result in lower grade talc metasomatism. However, the main control on formation of the banded oxide facies was the infiltration of Si- and Ca-bearing fluids along fractures in dolomite.

Massive Sulfide Facies

The massive sulfide facies (MSF) generally consists of pyrrhotite skarn with the mineral assemblage pyrrhotite ± sphalerite ± quartz ± fluorite ± chalcopyrite ± pyrite ± garnet ± pyroxene (Table 2). South of the Kuhn showing, sphalerite-rich skarn becomes dominant as a replacement of marble as well as early-formed skarn (Fig. 7d). Lateral zoning of iron minerals in the different skarn facies is a function of the relative concentrations of O_2 and S_2. The banded oxide (BO) facies reflects higher O_2 than the massive (MC) and banded (BC) calcsilicate facies, and all three facies are replaced by lower S_2 assemblages of the massive sulfide (MS) facies (Fig. 8d). Through reaction with the ore fluid, dolomite was a source of CO_2 (Nokleberg, 1973) and this increased O_2 in magnetite skarn. The concentration of S_2 was probably controlled by mixing of a relatively S_2-rich magmatic solution with a relatively S_2-poor formation fluid (see sulfur isotope discussion). However, the major control on metasomatic replacement of skarn was the infiltration of Fe- and S-bearing fluids along permeable zones in the other skarn facies.

SULFUR ISOTOPES

Sulfur isotopes were analyzed in 24 sulfide samples from McDame skarn, porphyry and hornfels (Table 4). Data are reported as delta values (δ), the per mil deviations of $^{34}S/^{32}S$ in the samples relative to that of the Canon Diablo meteorite standard. High levels of sample purity (99% mineral) and analytical precision (± 0.2 $\delta^{34}S$) were attained during sample preparation and analysis.

A plot of McDame sulfur isotope delta values (Fig. 9) shows that:

1) intrusive rock pyrite $\delta^{34}S$ (group 1) averages +4.7 (n=2), slightly heavier than magmatic $\delta^{34}S$ (0±3 from Ohmoto and Rye, 1979) but lighter than intrusive rock pyrrhotite $\delta^{34}S$ (group 5), which averages +9.3 (n=2);

2) country rock pyrrhotite $\delta^{34}S$ (group 6) averages +18.8 (n=2), much lighter than Cambrian sedimentary $\delta^{34}S$ (+30±3 from Faure, 1977);

3) skarn $\delta^{34}S$ for pyrite, pyrrhotite, sphalerite and chalcopyrite averages +7.7 (n=19) and forms three groups (2, 3, and 4) that lie between the intrusive rock and country rock data, and between the intrusive rock pyrite and pyrrhotite data;

4) skarn pyrite $\delta^{34}S$ (group 2) falls between +6.6 and +7.4 and averages +7.0 (n=6), with one exception ($\delta^{34}S$ = +8.2);

5) skarn pyrrhotite $\delta^{34}S$ (group 3) falls between +7.3 and +7.6 and averages +7.5 (n=6), with one exception ($\delta^{34}S$ = +5.0);

6) skarn pyrrhotite, sphalerite and chalcopyrite $\delta^{34}S$ from the massive calcsilicate and massive sulfide facies (group 4) falls between +8.1 and +8.7 and averages +8.4 (n=7); and

TABLE 4. Sulfur Isotope Data from Sulfides in Porphyry, Skarn and Hornfels

Sample Number	Rock Type	Mineral	d S
1029A	Kuhn stock: quartz feldspar porphyry	Pyrrhotite	+9.33
1075	Kuhn stock: quartz feldspar porphyry	Pyrite	+5.77
1077	Kuhn stock: quartz feldspar porphyry	Pyrrhotite	+9.35
1077	Kuhn stock: quartz feldspar porphyry	Pyrite	+3.72
81A5-144.35	Banded oxide facies skarn	Pyrite	+6.59
80A3-2555	Banded oxide facies skarn	Pyrite	+7.10
81A5-157.00	Banded oxide facies skarn	Pyrite	+6.96
81A5-157.00	Banded oxide facies skarn	Pyrrhotite	+7.53
1063A	Banded calcsilicate facies skarn	Pyrite	+7.11
1063A	Banded calcsilicate facies skarn	Pyrrhotite	+7.42
80A3-39.85	Massive calcsilicate facies	Pyrite	+7.37
80A3-39.85	Massive calcsilicate facies	Pyrrhotite	+7.47
1024E	Massive calcsilicate facies	Pyrite	+8.17
1024E	Massive calcsilicate facies	Pyrrhotite	+4.96
1066C	Massive calcsilicate facies	Pyrrhotite	+8.40
81A6-19.30	Massive calcsilicate facies	Pyrrhotite	+8.46
1064D	Massive sulfide facies	Pyrrhotite	+7.31
1064D	Massive sulfide facies	Sphalerite	+8.31
1064D	Massive sulfide facies	Chalcopyrite	+8.11
1110	Massive sulfide facies	Pyrrhotite	+7.58
1086	Massive sulfide facies	Pyrrhotite	+8.21
1071A	Massive sulfide facies	Pyrrhotite	+8.38
1074A	Massive sulfide facies	Pyrrhotite	+8.68
1080E	Kechika Group: graphitic hornfels	Pyrrhotite	+16.69
1047B	Atan Group: cordierite hornfels	Pyrrhotite	+20.87

1. Sulfur isotopes were analysed by C. Rees in the sulfur isotope laboratories at McMaster University; per mil deviations are relative to the Canon Diablo meteorite standard.

FIG. 9. Sulfur isotope plot for McDame data, showing the distribution of porphyry, skarn and hornfels $\delta^{34}S$ into six groups between ordinary magmatic and Cambrian sedimentary values: 1) porphyry pyrite $\delta^{34}S$ (n=2) averages +4.69 (x) ± 0.97 ($S/\sqrt{n}$); 2) skarn pyrite $\delta^{34}S$ (n=5) averages +7.03±0.13; 3) skarn pyrrhotite $\delta^{34}S$ (n=5) averages +7.46±0.05; 4) skarn pyrrhotite, sphalerite and chalcopyrite $\delta^{34}S$ (n=7) averages +8.36±0.07; 5) porphyry pyrrhotite $\delta^{34}S$ (n=2) averages +9.34±0.01; 6) hornfels pyrrhotite $\delta^{34}S$ (n=2) averages +18.78±2.96 . Five of six pyrite-pyrrhotite pairs are in reverse order to that expected from isotopic equilibrium. The exceptional pair (marked with star) gives an unrealistically low temperature of +34°C ($T = [550 / \sqrt{\delta^{34}SPY - \delta^{34}SPR}] - 273$, from Ohmoto and Rye, 1979) which also suggests isotopic disequilibrium.

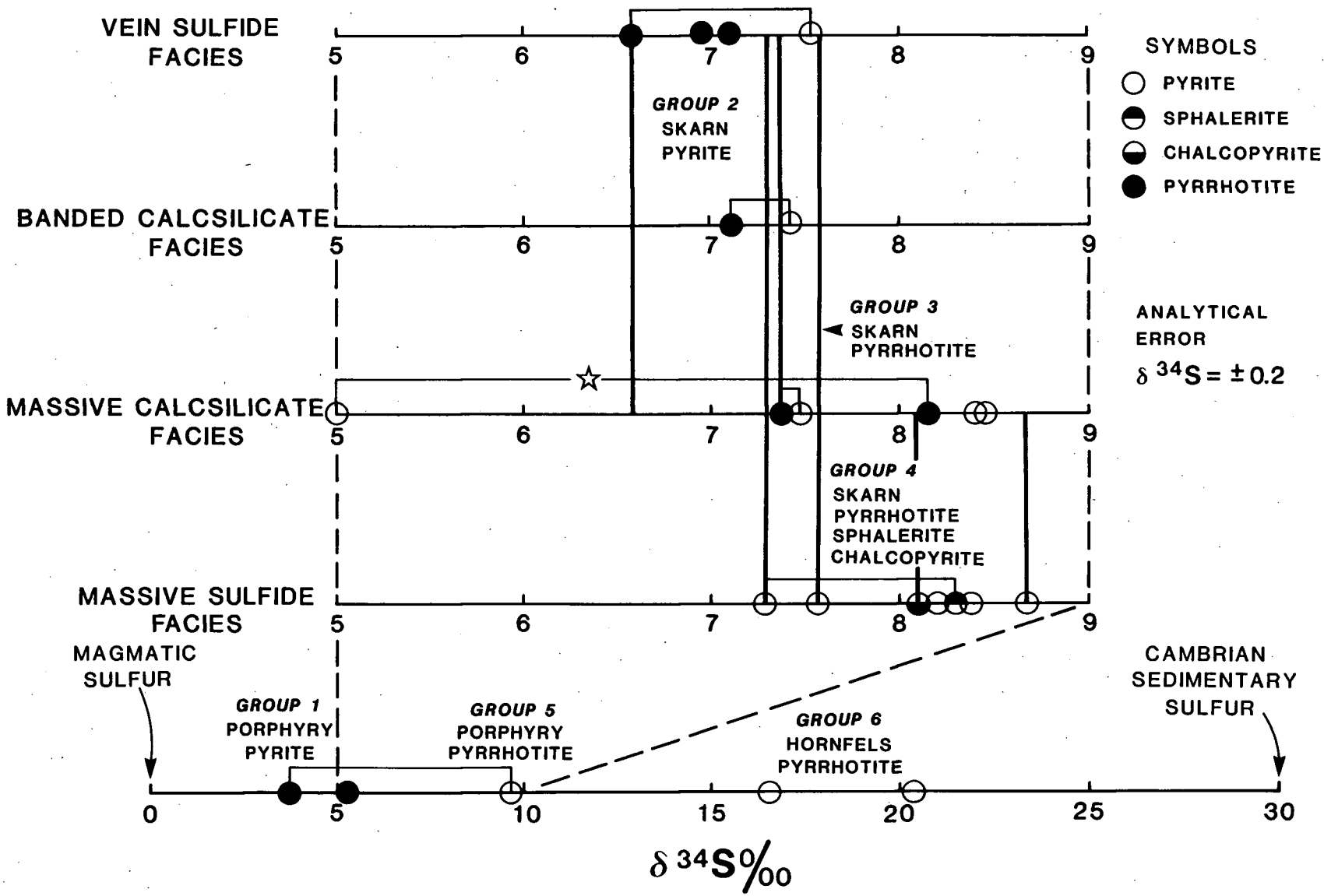

Fig. 9: Cooke and Godwin

7) in five of six pyrite-pyrrhotite pairs, pyrite $\delta^{34}S$ is lower than pyrrhotite $\delta^{34}S$, reverse to the order expected for isotopic equilibrium. Temperatures of mineralization calculated for the normal pyrite-pyrrhotite pair (34 °C) and a sphalerite-chalcopyrite pair (593 °C), using equations from Ohmoto and Rye (1979), are unrealistically low and high, respectively, again suggesting isotopic disequilibrium.

Primary disseminated pyrite in the Kuhn stock (group 1) probably reflects a granitic magma sulfur source whereas late pyrrhotite mineralization (group 5) and quartz alteration may represent mixing of sulfur from two sources. Intrusive rock pyrite ($\delta^{34}S$ = +4.7) is heavier than normal magmatic sulfur ($\delta^{34}S$ = 0) but this could be due to a relatively oxidizing and therefore SO_4^- and ^{34}S-rich magmatic fluid, buffered by ^{32}S-rich SH remaining in a relatively reducing magmatic melt (Ohmoto and Rye, 1979). Evidence for a Cambrian sedimentary sulfur source comes from the extensive bleaching, by destruction of graphite and pyrrhotite (group 6), of hornfels and dolomite associated with banded calcsilicate and banded oxide skarns. Country rock pyrrhotite ($\delta^{34}S$ = +18.8) is lighter than Cambrian sedimentary sulfate ($\delta^{34}S$ = +30) because the kinetic effects of bacterial or inorganic seawater sulfate reduction enrich sediments in ^{32}S (Faure, 1977).

Two sulfur sources are therefore indicated and both mixing and fractionation are necessary to explain the positive values of McDame sulfur isotopes and their present distribution between ordinary magmatic and Cambrian sedimentary values. Mixing of sulfur sources can also occur within granitic magmas by

assimilation of crustal rocks into mantle melts (Sasaki and Ishihara 1979; 1980) or by melting of sedimentary or igneous lower crust (Coleman, 1979). Intrusive rock pyrite may actually represent an isotopically heavy sulfur source for the Kuhn stock magma. However, a combined mixing-fractionation model predicts that:

1) upon intrusion and crystallization of the Kuhn stock, hot, acidic, oxidizing and sulfidizing magmatic waters moved upwards and outwards, precipitating pyrite (Fig.9, group 1: $\delta^{34}S$ = +4.7) in solidified intrusive rock (Fig. 10, point 1);

2) relatively cooler, more alkaline, reducing and less sulfidizing formational waters circulated in convection cells, dissolving pyrrhotite (Fig. 9, group 6: $\delta^{34}S$ = +18.8) from the country rocks;

3) progressive fractionation of sulfur isotopes and mixing of magmatic waters with up to 33% formational water along permeable contacts and faults produced the observed sulfur isotope ratio (Fig. 9, groups 2, 3, 4: $\delta^{34}S$ = +7.7) and sequence of ore facies in skarn (Fig. 10). Oxidation of graphite, dissolution of calcite, precipitation of sulfides and a reservoir effect due to country rocks becoming depleted in ^{34}S all tend to decrease T, aO_2, aS_2 and aH_2 in the ore fluid resulting in its progressive enrichment in ^{34}S and H_2S (Fig. 10).

4) skarn pyrite (Fig. 9, group 2: $\delta^{34}S$ = +7.0), magnetite and molybdoscheelite precipitated in the banded oxide, banded calcsilicate and massive calcsilicate facies from a relatively small but ^{34}S-rich H_2S fraction in the still dominantly hot and

FIG. 10. Partial T-aO_2 diagram for the system SiO_2-Fe_2O_3-FeO-FeS-FeS_2- O_2-S_2-H_2 at P = 1000 bars (Ohmoto and Rye, 1979), showing, by dashed lines, selected ore mineral equilibria (13) $SO_2 + H_2O = H_2S + 2O_2$, (14) 6HE = 4MG + O_2, (15) MG + 3PY = 6PR + $2O_2$, (16) 2MG + 3QZ = 3FY + O_2, and, by solid lines, $\delta^{34}S$ values for H_2S in the ore fluid. Mineral symbols are defined in Table 2. Porphyry pyrite (group 1) precipitated from a hot (T = 650°C), oxidizing (log aO_2 = -15) magmatic ore fluid, which fractionated with decreasing T (500°C) and aO_2 (-21) to produce skarn pyrite (group 2) and pyrrhotite (group 3). Mixing of magmatic water with cooler, more reducing formational water at lower T (350°C) and log aO_2 (-32) resulted in replacement of earlier skarns by pyrrhotite, sphalerite and chalcopyrite (group 4) and mineralization of porphyry by pyrrhotite (group 5).

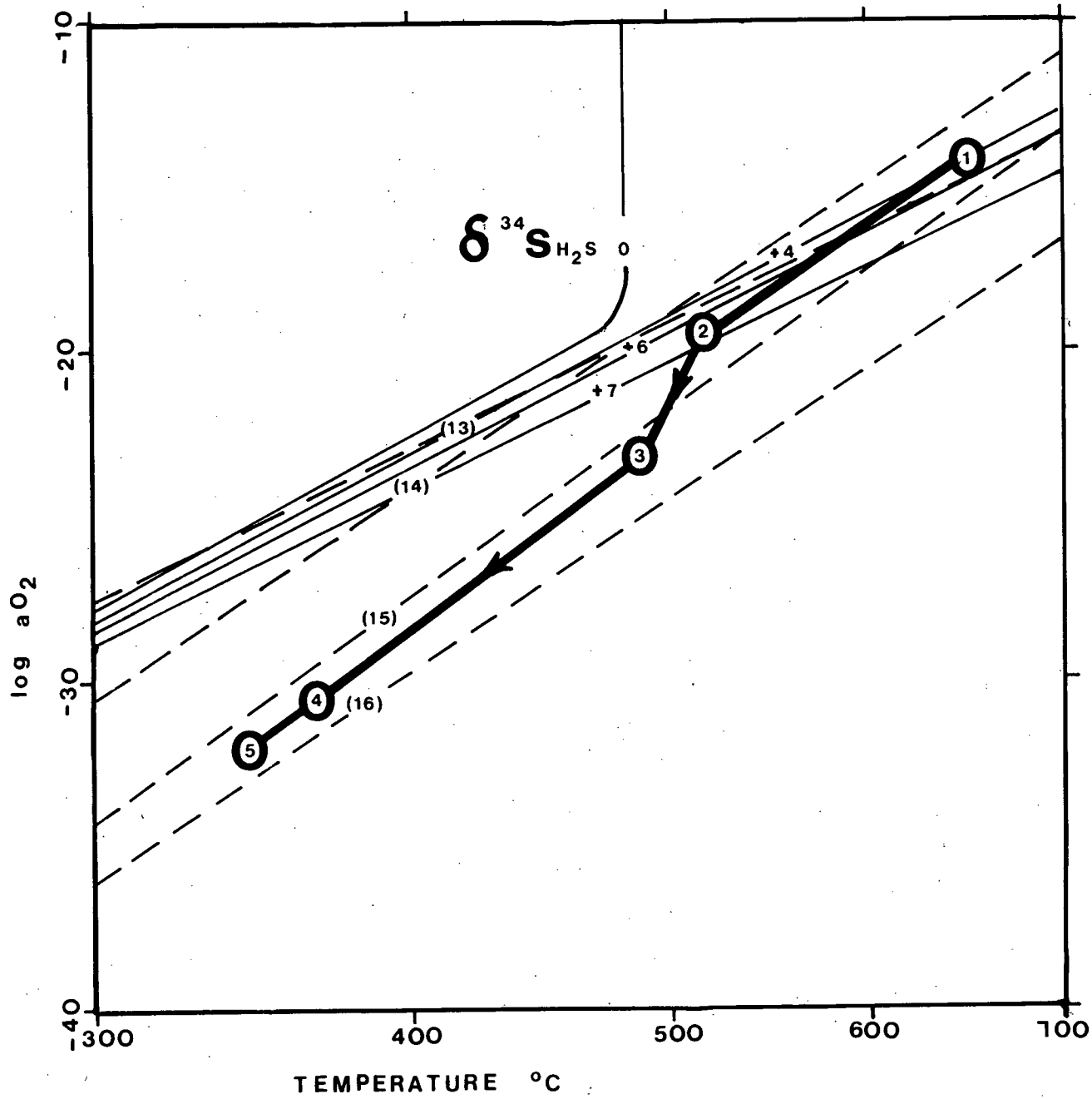
-10
-20
-30
-40
log aO_2
$\delta^{34}S_{H_2S}$ 0
+4
+6
+7
(13)
(14)
(15)
(16)
1
2
3
4
5
-300
400
500
600
700
TEMPERATURE °C

oxidizing magmatic ore fluid (Fig. 10, point 2);

5) skarn pyrrhotite associated with pyrite (Fig. 9, group 3: $\delta^{34}S$ = +7.5), scheelite and molybdenite were deposited in the massive calcsilicate facies from a less hot and oxidizing magmatic ore fluid (Fig. 10, point 3);

6) skarn pyrrhotite, sphalerite, chalcopyrite (Fig. 9, group 4: $\delta^{34}S$ = +8.4) and scheelite in massive sulfide facies formed from a more cool and reducing mixed magmatic and formational ore fluid (Fig. 10, point 4); and

7) collapse of the hydrothermal system resulted in final mineralization of pyrrhotite (Fig. 9, group 5: $\delta^{34}S$ = +9.3) and quartz alteration in the intrusive rocks themselves (Fig. 10, point 5).

Comparison of McDame sulfur isotope data with those of other tungsten skarns shows that $\delta^{34}S$ values fall in a very narrow range for each deposit. At Moina, Tasmania, $\delta^{34}S$ of pyrite, pyrrhotite and sphalerite range from +8.4 to +9.3 (Kwak and Askins, 1981). Shimazaki and Yamamoto (1979) report $\delta^{34}S$ values for pyrite, pyrrhotite, sphalerite, galena and chalcopyrite in tungsten deposits of Japan, including Kagata mine (-1.3 to -1.1), Tsumo mine (-1.7 to +0.7), Kawayama mine (-6.3 to -4.6, Kuga mine (-9.2 to -8.3), Fujigatani mine (-12.2 to -6.9), and Kiwada mine (-8.5 to -7.1). Pyrite $\delta^{34}S$ values from the Osgood Mountains, Nevada (Taylor and O'Neil, 1977) range from +5.4 to +6.7 (Marcus mine), +2.0 to +4.6 (Kirby mine), +1.5 to +3.2 (Alpine mine) and around +2.4 (Riley extension mine). Since high temperature is a unique feature of skarn deposits relative to other hydrothermal deposits, it must be a primary

control on the relatively minor sulfur isotope fractionation in skarns, as shown by their narrow variation in $\delta^{34}S$.

RUBIDIUM-STRONTIUM ISOTOPES

Rubidium-strontium and potassium-argon ages were determined from a 25 kg sample of Kuhn stock quartz feldspar porphyry. The stock typically is porphyritic with 10% phenocrysts of corroded quartz, 20% megacrysts of perthite mantled by albite, and 15% glomerocrysts of plagioclase showing oscillatory, normal zoning (An_{15} to An_{25}). Quartz, feldspar and biotite form a fine grained matrix containing traces of muscovite, chlorite, sphene, apatite, zircon, calcite, pyrite and magnetite (Table 2).

Potassium-argon dating of biotite (Table 5) gives a Late Cretaceous age of 72.4 ± 2.5 Ma, concordant with a rubidium-strontium whole rock(WR) - biotite(BI) isochron of 69 ± 2 Ma which has an initial strontium isotope ratio of 0.712 (Table 6 and Fig. 11). Similar Late Cretaceous ages have been obtained from the nearby Cassiar stock by Christopher et al. (1972) and Panteleyev (1980). An older isochron of 139 ± 16 Ma with an initial $^{87}Sr/^{86}Sr$ ratio of 0.709 is given by the whole rock - light matrix feldspar(LF) - heavy matrix feldspar(HF) - megacrystic perthite(KF) system (Fig. 11) indicating that it is not in equilibrium with the whole rock-biotite system. Such disequilibrium has been interpreted as evidence for progressive contamination of a mantle melt by crustal material during magma ascent and crystallization (Schuler and Steiger, 1978). Hence, subtraction of these less radiogenic components from the whole rock analysis should produce a slightly younger isochron and

TABLE 5. Potassium-Argon Isotope Data from Quartz Feldspar Porphyry of the Kuhn Stock

Sample Number	Location Lat(N)	Long(W)	Rock Unit, and Rock Name	Mineral Dated	%K	Ar* Ar total	Ar* 10^{-6} cm STP/g	Apparent Age (Ma)	Time
1075	59.34	129.85	Kuhn stock, quartz feldspar porphyry	Biotite	6.50	0.921	1.867	72.4±2.5	Late Cretaceous

1. Argon analyses were done by J. Harakal and K. Scott did the potassium analyses. All analyses were done at the Geochronology Laboratory, The University of British Columbia.
2. Ar* indicates radiogenic argon.
3. Constants used are from Steiger and Jager (1977): $=0.581 \times 10$ yr ; $=4.962 \times 10$ yr ; $K/K=1.162 \times 10$.
4. Time designation is from Armstrong (1978).

TABLE 6. Rubidium-Strontium Isotope Data from Quartz Feldspar Porphyry of the Kuhn Stock

Sample Number	Location Lat(N)	Long(W)	Rock Unit and Rock Name	Material Analysed	Sr(ppm)	Rb(ppm)	$^{87}Sr/^{86}Sr$	$^{87}Rb/^{86}Sr$
1075WR	59.34	129.85	Kuhn stock, quartz feldspar porphyry	Whole rock	287	265	0.7141	2.68
1075BI	59.34	129.85	Kuhn stock, quartz feldspar porphyry	Biotite	35.0	859	0.7820	71.6
1075KF	59.34	129.85	Kuhn stock, quartz feldspar porphyry	K-feldspar megacryst	504	108	0.7104	0.623
1075HF	59.34	129.85	Kuhn stock, quartz feldspar porphyry	Heavy matrix feldspar	233	122	0.7117	1.51
1075LF	59.34	129.85	Kuhn stock, quartz feldspar porphyry	Light matrix feldspar	292	250	0.7143	2.48

1. All analyses by K. Scott, Geochronology Laboratory, Department of Geological Sciences, The University of British Columbia.

FIG. 11. Rubidium-strontium isotope plot for minerals from the Kuhn stock (Fig. 2), showing a biotite (BI)-whole rock (WR) isochron that gives an initial $^{87}Sr/^{86}Sr$ ratio of 0.712 and a date of 69 ± Ma. The whole rock-light matrix feldspar (LF)-heavy matrix feldspar (HF)-megacryst perthite (KF) system produces an older isochron (139 ± 16 Ma) with a lower initial $^{87}Sr/^{86}Sr$ ratio (0.709), indicating that it is out of equilibrium with the whole rock-biotite system. Such disequilibrium suggests progressive contamination of a granitic melt by sialic crust during magma crystallization. The high initial strontium isotope ratio indicates that the Kuhn stock magma had a sialic crustal component.

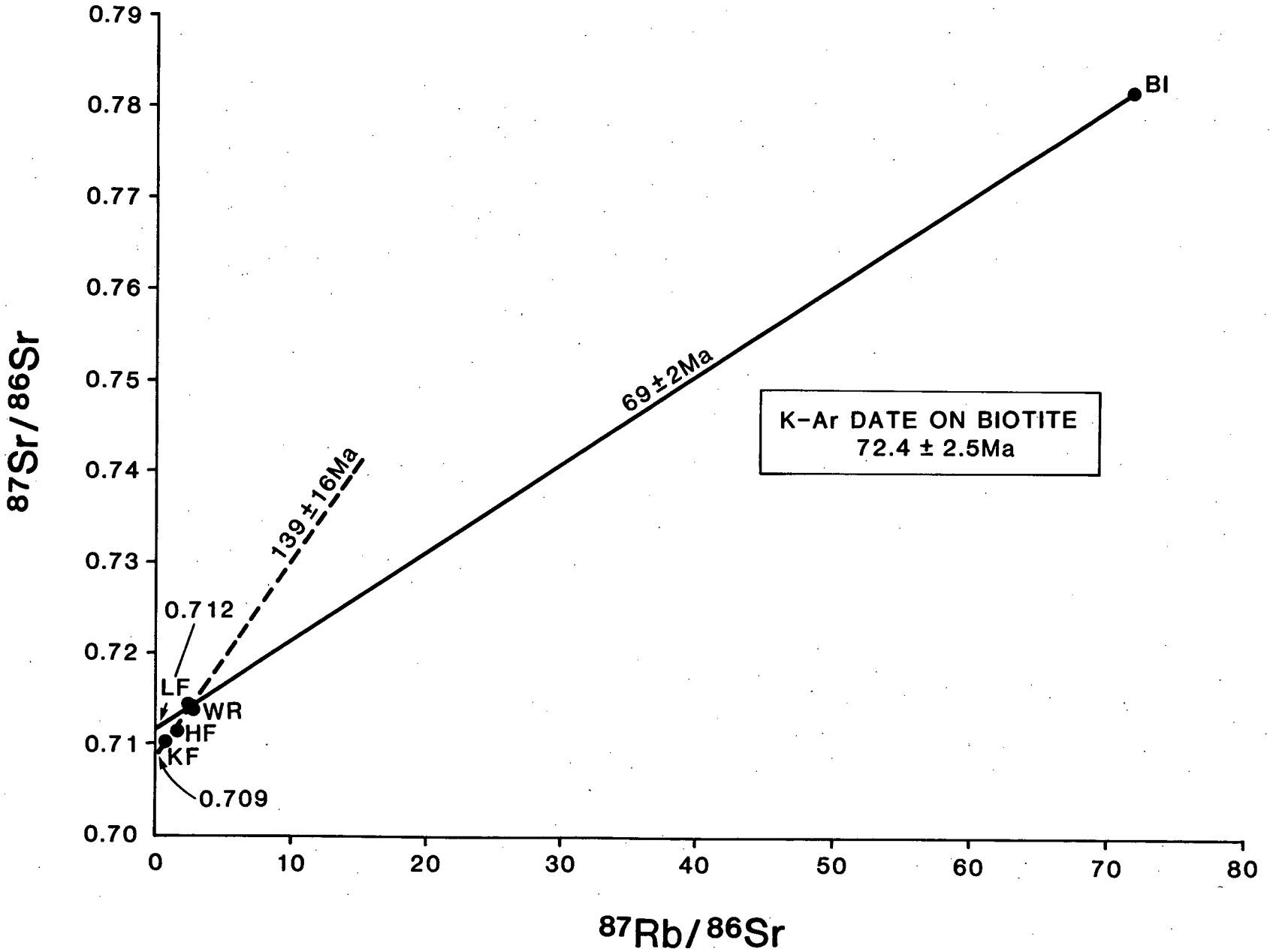
0.79
0.78
0.77
0.76
0.75
0.74
0.73
0.72
0.71
0.70
87Sr/86Sr
0
10
20
30
40
50
60
70
80
87Rb/86Sr
BI
69±2Ma
139±16Ma
K-Ar DATE ON BIOTITE
72.4 ± 2.5Ma
0.712
LF
WR
HF
KF
0.709

higher initial $^{87}Sr/^{86}Sr$ ratio (Godwin et al., 1980).

High initial $^{87}Sr/^{86}Sr$ ratios (>0.706) characterize granitic rocks derived by melting and/or assimilation of old sialic crust during magma genesis and low initial ratios (<0.704) indicate mantle and/or young simatic crustal source (Faure, 1977). Thus, the Kuhn stock magma (0.712) probably had a sialic crustal component. Similar high initial $^{87}Sr/^{86}Sr$ ratios have been obtained from other Cretaceous granitic plutons in the Omenica Crystalline and Rocky Mountain Belts of Figure 1 (<0.710 from Fairbairn et al., 1964; 0.725 from Wanless et al., 1968; 0.723 from Godwin et al., 1980; 0.712 from Kuran et al., 1982; 0.712 from Mato et al., 1983; and 0.725 from Armstrong, 1983). Radiogenic Sr in these intrusions implies that Precambrian continental crust underlay the eastern Canadian Cordillera during Cretaceous time. In the more western Intermontane, Coast Plutonic and Insular Belts (Fig. 1), underlain by younger oceanic crust, felsic intrusions have initial strontium isotope ratios lower than 0.706 (Le Couteur and Tempelman-Kluit, 1976; Morrison et al., 1979; Anderson et al., 1983).

Metamorphosed miogeoclinal sediments of the Omenica Crystalline Belt have been displaced from similar unmetamorphosed rocks in the Rocky Mountain Belt by more than 1000 km of right lateral strike slip movement during late Cretaceous to early Tertiary time (Gabrielse, 1983). Isotopic evidence suggests that stocks intruding Rocky Mountain Belt sediments have higher initial $^{87}Sr/^{86}Sr$ ratios than batholiths intruding Omenica Crystalline Belt metasediments. Higher initial strontium isotope ratios, smaller size of intrusive bodies and

lower grade regional metamorphism of country rocks coincide with greater crustal thickening in the Rocky Mountain Belt than in the Omenica Crystalline Belt (Armstrong, 1983). Rocky Mountain Belt plutons therefore have a greater lithophile component than Omenica Crystalline Belt intrusions and hold more potential to produce tungsten skarn deposits.

LEAD ISOTOPES

Lead isotope ratios were measured for galena from seven silver or gold veins and one tungsten skarn (Table 7). These deposits are related closely to the felsic intrusions near Cassiar (Fig. 1). Lead ratios cluster on the upper crustal "shale" curve that is generally applicable to the Omineca Crystalline Belt in the Canadian Cordillera (Godwin and Sinclair, 1982; Andrew et al., 1983; 1984); a $^{206}Pb/^{204}Pb$ model age, based on the shale curve, from the average and standard deviation in Table 7, yields an Early Cretaceous age of 137 ± 24 Ma. Although the precision of this age is poor, compared to other methods described above, the lead clearly has an upper crustal source rather than a mantle or lower crustal source. If the source of the lead is from the intrusions this would be in agreement with the rubidium-strontium interpretation that assimilated crustal rocks formed an important component of intrusions in the Cassiar area.

INTRUSION CHEMISTRY

On the basis of accessory muscovite, normative corundum, $K_2O > Na_2O$, $Al_2O_3 > K_2O+Na_2O+1/2CaO$ and $^{87}Sr/^{86}Sr > 0.712$ (Table

TABLE 7: Galena-Lead Isotope Analyses From Gold or Silver Veins and Tungsten Skarn

Sample Number	Anal-yst	Deposit Name	Map Name	Lat. North	Long. West	Lead Isotope Ratios (Relative 1S Error as %) 206/204	207/204	208/204	Remarks
30383-001	1	Coast Silver	383	59.26	129.83	19.243 (.07)	15.682 (.15)	39.416 (.14)	Ven. Atan Gp MARB
30384-001	1	Ray 2	384	59.27	129.85	19.199 (.03)	15.667 (.09)	39.309 (.13)	Ven. Atan Gp MARB
30385-001	1	Lower Granite Ck: D-Zone	385	59.28	129.82	19.326 (.08)	15.770 (.15)	39.571 (.15)	Ven. Atan Gp DOLM
30386-001	1	Weiseman	386	59.13	129.77	19.224 (.02)	15.735 (.09)	39.349 (.04)	Ven. Ingenika MARB
30387-001#	1	Contact - Telemac	387	59.32	129.87	18.990 (.18)	15.666 (.25)	39.222 (.33)	Ven. Ingenika MARB
30387-002	1	Contact - Telemac	387	59.32	129.87	19.317 (.20)	15.808 (.45)	39.582 (.30)	Ven. Ingenika MARB
30399-001	1	Skarn Showing	399	59.33	129.88	19.272 (.07)	15.700 (.17)	39.360 (.17)	Skr. Ingenika LIMS
30400-001	1	Cusac	400	59.19	129.70	19.271 (.07)	15.709 (.12)	39.256 (.13)	Ven. Sylvest. VOLC
SUMMARY: CASSIAR MINERAL OCCURRENCES		Arithmetic average (x̄) =				[19.265]	[15.727]	[39.406]	
Number of deposits (n) = [7]		Standard deviation (S) =				[0.047]	[0.051]	[0.126]	
Number of analyses (a) = [8]		Std. error of mean ($S_{\bar{x}}$) =				[0.018]	[0.019]	[0.048]	

1. All analyses, by B. Ryan, were done in the Geology-Geophysics Laboratory, The University of British Columbia.
2. Analysis marked with an "#" was deleted from calculations because of suspected poor quality.
3. Abbreviations used in remarks are: Gp = Group, Ingenika = Ingenika Group, Sylvest. = Sylvester Group, Skr. = skarn, Ven. = vein, DOLM = dolomite, LIMS = limestone, MARB = marble, and VOLC = volcanics.

7), the Kuhn and Cassiar stocks are classified as S-type granites (Chappell and White, 1974) formed by anatexis of sedimentary rocks. Such an origin is consistent with the melting of continental crust to produce a granitic magma (White and Chappell, 1977; White et al., 1977), but differentiation of a magma from an igneous source rock can also produce a granite with similar chemical trends (Chappell, 1979).

Accessory magnetite and pyrite > 0.1%, magnetic susceptibility > 0.0004 emu/g, and $\delta^{34}S > 0$ (Table 8) indicate that the Kuhn and Cassiar stocks also conform to magnetite-series granites (Ishihara, 1977) that formed from relatively oxidizing magmas. Ishihara (1981) notes that in Australia, magnetite-series granites correlate only with I-type intrusions whereas ilmenite-series plutons can form from magmas of either S- or I-type origin. However, an oxidizing magma does not preclude derivation of the Kuhn and Cassiar stocks from a source rock of mixed or sedimentary provenance. Both Ishihara (1977) and Chappell and White (1974) suggest that tungsten skarn and porphyry molybdenum ore deposits are more typical of I-type and magnetite-series granitic plutons than S-type and ilmenite-series granitoids. In contrast, the McDame W skarn and Casmo Mo porphyry deposits (Panteleyev, 1979) are related to S-type and magnetite-series granites, indicating that both sedimentary source rocks and differentiation of an oxidizing magma were important at Cassiar.

Anomalously high K_2O, K/Rb, U and U/Th (Table 7) indicate that the Kuhn stock is geochemically specialized (Tischendorf, 1977) in these radioactive elements. Although not specialized in

TABLE 8: Chemistry and Mineralogy of the Cassiar Intrusions

	CASSIAR	KUHN 1	KUHN 2	S TYPE	M TYPE	SPECIALIZED
MAJOR ELEMENTS %						
SiO	68.0	66.0	68.5	68.07	75.40	73.38
TiO	0.54	0.71	0.62	0.63	0.13	0.16
Al O	14.3	14.8	14.1	14.49	13.29	13.97
Sum FeO	2.92	3.06	2.45	4.40	1.41	1.90
MnO	0.08	0.05	0.03	0.07	0.04	0.05
MgO	1.01	1.28	0.88	2.13	0.43	0.47
CaO	1.98	2.11	1.45	2.55	1.30	0.75
Na O	3.54	3.55	3.16	2.07	3.51	3.20
K O	4.09	4.58	5.20	3.30	3.93	4.69
P O	0.21	0.23	0.23	0.15	0.05	-
LOI	0.77	1.16	1.00	1.93	0.47	-
TOTALS	97.44	97.53	97.62	99.79	99.96	98.57
TRACE ELEMENTS ppm						
Rb	240	-	265	169	-	550
Sr	214	-	287	129	-	100
U	8	-	11	3	-	-
Th	30	-	35	18	-	-
W	2	-	4	-	-	7
Mo	2	-	6	-	-	3.5
Sn	2	-	1	-	-	30
F	532	-	583	-	-	3180
Li	55	-	29	-	-	400
Be	4	-	4	-	-	13
ELEMENT RATIOS						
Al O /(K O+Na O+1/2CaO)	1.7	1.6	1.6	2.2	1.6	1.7
K O/Na O	1.2	1.3	1.5	1.6	1.1	1.5
K/Rb	141	-	163	162	-	71
Rb/Sr	1.1	-	0.9	1.3	-	5.5
U/Th	0.3	-	0.3	0.2	-	-
Mg/Li	110	-	182	-	-	7.1
NORMATIVE MINERALS %						
Quartz	26.43	21.82	26.62	33.38	35.97	33.79
Orthoclase	25.01	28.10	31.82	19.91	23.34	28.11
Albite	30.18	30.39	27.01	17.85	29.83	27.46
Anorthite	8.75	9.31	5.89	11.92	6.15	3.77
Hypersthene	6.26	6.84	4.98	11.07	3.01	3.84
Corundum	1.15	0.90	1.36	3.31	1.03	2.30
Apatite	0.50	0.55	0.55	0.35	0.12	0.00
Ilmenite	1.06	1.40	1.22	1.22	0.25	0.31
Magnetite	0.66	0.69	0.55	0.98	0.31	0.42
MODAL MINERALS %						
Quartz	40	35	40	44	-	35
K-Feldspar	15	20	25	5	-	33
Plagioclase	35	35	30	33	-	25
Biotite	8	7	5	18	-	3
Muscovite	0	1	3	0	-	3
Chlorite	1	1	1	0	-	0
Sphene	<1	<1	<1	0	-	0
Apatite	<1	<1	<1	0.1	-	0
Zircon	<1	<1	<1	0.1	-	0
Magnetite	0	<1	<1	0.2	-	1
Pyrite	0	<1	1	-	-	-
MAGNETIC SUSCEPTIBILITY emu/g x 10	17	4.2	8.6		>1	

1. Chemical analyses by Chemex Labs Ltd., Vancouver, B.C. Mineral modes are from visual estimates of thin sections. CIPW norms are calculated using standardized FeO-Fe O ratios (Brooks, 1976). Magnetic susceptibility was measured on pulverized samples.
2. Data, sample BB34, are from White et al. (1977).
3. Data, average of nine samples, are from Tanaka and Nozawa (1977). Magnetite content is greater than 0.1 volume percent in M-Type granitoids (Ishihara, 1981).
4. Data, average of 962 samples, are from Tischendorf (1977).

W or Mo relative to a world average, the Kuhn stock does contain more W and Mo than the Cassiar stock (Table 7) and therefore holds greater potential to produce W-Mo skarns. Strong (1981) notes that biotite quartz monzonites are generally barren of mineralization whereas more differentiated felsic plutons form granophile Sn-W-U-Mo ore deposits and less differentiated mafic plutons form porphyry Cu-Mo ore deposits. However, tungsten skarns in the Canadian Cordillera are uniquely associated with biotite quartz monzonites (Dick and Hodgson, 1982) and the Kuhn stock is a biotite quartz monzonite (Strecheisen, 1974) of calcalkaline affinity (Irvine and Baragar, 1971). Thus, something other than magmatic differentiation must influence the mineralizing potential of a granitic pluton. Accounting for a magma's source rock as well as its differentiation history may help to evaluate the potential for mineral deposits associated with acidic intrusions. A simple model for the origin of granitic plutons and ore minerals at McDame thus includes:

1) a sialic crustal source to the Cassiar and Kuhn stocks and their lithophile elements through melting of lower crust and/or assimilation of upper crust;

2) magmatic differentiation and geochemical specialization of an oxidizing magma to produce Al_2O_3-K_2O-U rich granitic plutons and W-Mo skarn deposits.

CONCLUSIONS

1) The McDame tungsten skarn prospect is contained in Lower Hadrynian to Lower Ordovician clastic and carbonate metasediments of the Ingenika, Atan and Kechika Groups where

they are intruded by felsic stocks of the Cassiar Intrusions. The Cassiar area has been offset along the Tintina and related faults from a world class tungsten skarn district in similar unmetamorphosed rocks of the Rocky Mountain Belt. Therefore, Omenica Crystalline Belt rocks near Cassiar hold potential to host economic tungsten skarns.

2) Four metasomatic facies at McDame are lithologically and structurally controlled. Prograde massive calcsilicate W-Mo-Fe, banded calcsilicate Fe, banded oxide W-Mo-Fe and retrograde massive sulfide Fe-Zn-Cu-W skarns replace marble, hornfels, dolomite and skarn, respectively, along contacts, fractures and faults. Only the massive calcsilicate facies attains ore thickness and grade but the banded calcsilicate and oxide facies are useful in mineral exploration because they signal the presence of buried felsic intrusions.

3) An estimated lithostatic pressure of 1500 bars suggests formation of McDame skarns at about six kilometers depth. Temperatures for prograde skarn was about 500°C at CO_2 mole fractions less than 0.15. Retrograde skarn formed at lower T and XCO_2.

4) Calcsilicate mineral zoning resulted from dissolution, infiltration/diffusion and deposition of SiO_2, CaO, Al_2O_3, MgO, H_2O and CO_2 in marble, dolomite and hornfels by magmatic fluids. Higher grade minerals such as garnet in quartz skarn and plagioclase in magnetite skarn signal proximity to a felsic intrusion (within tens of meters). Metallic mineral zoning was formed by infiltration of relatively W-, Mo- O_2- and S_2-rich magmatic fluids and mixing with relatively Fe-, Zn- and Cu-rich,

O_2- and S_2-poor formational waters along permeable zones in skarn. This zoning is useful in guiding mineral exploration from distal sphalerite- and chalcopyrite-rich skarns to more proximal scheelite- and molybdenite-rich skarns.

5) Sulfur isotope data suggest that fractionation of magmatic sulfur ($\delta^{34}S = 0$) produced porphyry pyrite ($\delta^{34}S = +4.7$), skarn pyrite ($\delta^{34}S = +7.0$) and skarn pyrrhotite ($\delta^{34}S = +7.5$) and mixing with formational sulfur formed skarn pyrrhotite-sphalerite-chalcopyrite ($\delta^{34}S = +8.4$) and porphyry pyrrhotite($\delta^{34}S = +9.3$). High temperature of skarn formation results in the relatively minor fractionation of sulfur isotopes and the narrow variations in $\delta^{34}S$.

6) Rubidium-strontium and lead isotopes indicate that the Kuhn stock had a strong sialic component from melting and/or assimilation of continental crust. Thus, differentiation of an oxidizing, crustally derived magma enriched in lithophile elements produced the McDame tungsten skarn deposit. Higher initial strontium isotope ratios from Cretaceous felsic plutons in the Rocky Mountain Belt suggest that they hold more potential to produce tungsten skarns than similar, younger intrusions in the Omenica Crystalline Belt.

REFERENCES

Anderson, R.G., Armstrong, R.L., Parrish, R. and Bowman, J.R., 1983, Potential of SE Selwyn Plutonic Suite for W skarn deposits: Geological Association Canada, Programme with Abstracts, v.8, p.A2.

Andrew, A., Godwin, C.I., and Sinclair, A.J., 1983, A new interpretation of lead data from Moyie, Slocan, Carmi, and Ainsworth-Bluebell camps, southeastern British Columbia: Geological Association Canada, Programme with Abstracts, v.8, p.A2.

Andrew, A., Godwin, C.I., and Sinclair, A.J., 1984, Mixing line isochrons: a new interpretation of galena lead isotope data from southeastern British Columbia: Economic Geology, this issue.

Armstrong, R.L., 1978, Pre-Cenozoic Phanerozoic Time Scale--computer file of critical dates and consequences of new and in-progress decay constant revisions: in, Contributions to the Geologic Time Scale, ed. G.V. Cohee, M.F. Glaessner, and H.D. Hedberg, American Association Petroleum Geologists, Studies in Geology No. 6, p.73-92.

Armstrong, R.L., 1983, Cordilleran S- and I-type granites: Indicators of lithosphere thickness: Geological Association Canada, Programme with Abstracts, v.8, p.A3.

Brooks, C.K., 1976, The Fe_2O_3 ratio of basalt analyses: an appeal for a standardized procedure: Bulletin Geological Society Denmark, v.25, p.117-120.

Chappell, B.W., 1979, Granites as images of their source rocks: Geological Society America, Abstracts with Programs, v.11, p.400.

Chappell, B.W. and White, A.J.R., 1974, Two contrasting granite types: Pacific Geology, v.8, p.173-174.

Christopher, P.A., White, W.H. and Harakal, J.E., 1972, Age of tungsten and molybdenum mineralization in northern British Columbia: Canadian Journal Earth Sciences, v.9, p.1727-1734.

Coleman, M.L., 1977, Sulfur isotopes in petrology: Journal Geological Society London, v.133, p.593-608.

Cooke, B.J. and Godwin, C.I., 1982, Geology of the McDame tungsten skarn prospect: British Columbia Ministry Energy, Mines, Petroleum Resources, Paper 1982-1, p.259-269.

Crawford, M.L.,1981, Phase equilibria in aqueous fluid inclusions: Mineralogical Association Canada, Short course in fluid inclusions: Applications to petrology, ed. L.S. Hollister and M.L. Crawford, Chapter 4, p.75-100.

Dick, L.A. and Hodgson, C.J., 1982, The Mactung W-Cu(Zn) contact metasomatic and related deposits of the northeastern Canadian Cordillera: Economic Geology, v.77, p.845-867.

Fairbairn, H.W., Hurley, P.M. and Pinson, W.H., 1964, Initial

$^{87}Sr/ ^{86}Sr$ and possible sources of granitic rocks in southern British Columbia: Journal Geophysical Research, v.69, n.22, p.4889-4893.

Faure, G., 1977, Principles of isotope geology: John Wiley and Sons, 464p.

Fritz, W.H., 1978, Upper (carbonate) part of Atan Group, Lower Cambrian, north-central British Columbia: Geological Survey Canada, Paper 78-1A, p.7-16.

Fritz, W.H., 1980, Two new formations in the Lower Cambrian Atan Group, Cassiar Mountains, north-central British Columbia: Geological Survey Canada, Paper 80-1B, p.217-225.

Gabrielse, H., 1963, McDame map-area, Cassiar district, British Columbia: Geological Survey Canada, Memoir 319, 138p.

Gabrielse, H., 1983, Major transcurrent displacements along the northern Rocky Mountain trench and related lineaments in north-central British Columbia: Geological Survey Canada, Paper 83-8, p.1.

Godwin, C.I., Armstrong, R.L. and Tompson, K.M., 1980, Geology, K-Ar and Rb-Sr dating of the Clea Tungsten Skarn Property, Selwyn Mountains, Yukon Territory: Canadian Institute Mining Metallurgy, Bulletin, v.75, n.821, p.90-93.

Godwin, C.I. and Sinclair, A.J., 1982, Average lead isotope growth curve for shale-host zinc-lead deposits, Canadian Cordillera: Economic Geology, v.77, p.675-690.

Helgeson, H.C., Delany, J.M., Nesbitt, H.W., and Bird, D.K., 1978, Summary and critique of the thermodynamic properties of rock-forming minerals: American Journal Science, v.278A, 229p.

Irvine, T.N., and Baragar, W.R.A., 1971, A guide to the chemical classification of the common volcanic rocks: Canadian Journal Earth Sciences, v.8, p.523-548.

Ishihara, S., 1977, The magnetite-series and ilmenite-series granitic rocks: Mining Geology, v.27, p.293-305.

Ishihara, S., 1981, The granitoid series and mineralization: Economic Geology, 75th Anniversary Volume, p.458-484.

Korzhinskii, D.S., 1970, Theory of metasomatic zoning: Clarendon Press, 162p.

Kuran, V.M., Godwin, C.I. and Armstrong, R.L., 1982, Geology and geochronometry of the Scheelite Dome tungsten-bearing skarn property, Yukon Territory: Canadian Institute Mining Metallurgy, Bulletin, v.75, n.838, p.137-142.

Kwak, T.A.P. and Askins, P.W., 1981, Geology and genesis of the F-Sn-W(-Be-Zn) skarn (wrigglite) at Moina, Tasmania: Economic

Geology, v.76, p.439-467.

Le Couteur, P.C. and Tempelman-Kluit, D.J., 1976, Rb/Sr ages and a profile of $^{87}Sr/^{86}Sr$ ratios for plutonic rocks across the Yukon Crystalline Terrane: Canadian Journal Earth Sciences, v.13, p.319-330.

Mansy, J.L., 1979, Stratigraphy and structure of Proterozoic rocks near Good Hope Lake, McDame map-area, British Columbia: Geological Survey Canada, Paper 78-1A, p.5-6.

Mansy, J.L. and Gabrielse, H., 1978, Stratigraphy, terminology and correlation of Upper Proterozoic rocks in Omenica and Cassiar Mountains, north-central British Columbia: Geological Survey Canada, Paper 77-19, 17p.

Mato, G., Ditson, G. and Godwin, C.I., 1983, Geology and geochronometry of tin mineralization associated with the Seagull batholith, south-central Yukon Territory: Canadian Institute Mining Metallurgy, Bulletin, v.76, n.854, p.43-49.

Monger, J.W.H. and Price, R.A., 1979, Geodynamic evolution of the Canadian cordillera - progress and problems: Canadian Journal Earth Sciences, v.16, p.770-791.

Monger, J.W.H., Souther, J.G. and Gabrielse, H., 1972, Evolution of the Canadian Cordillera - a plate tectonic model: American Journal Science, v.272, p.577-602.

Monger, J.W.H., Price, R.A. and Tempelman-Kluit, D.J., 1982, Tectonic accretion and the origin of the two major metamorphic and plutonic welts in the Canadian Cordillera: Geology, v.10, p.70-75.

Morrison, G.W., Godwin, C.I. and Armstrong, R.L., 1979, Interpretation of isotopic ages and $^{87}Sr/^{86}Sr$ initial ratios for plutonic rocks in the Whitehorse map-area, Yukon: Canadian Journal Earth Sciences, v.16, p.1988-1997.

Nokleberg, W.J., 1973, CO_2 as a source of oxygen in the metasomatism of carbonates: American Journal Science, v.273, p.498-514.

Ohmoto, H. and Rye, R.O., 1979, Isotopes of sulfur and carbon: in, Geochemistry of Hydrothermal Ore Deposits, Vol. II, ed. H.L. Barnes, Chapter 10, p.509-567.

Panteleyev, A., 1979, Cassiar map-area: British Columbia Ministry Energy, Mines, Petroleum Resources, Paper 1979-1, p.51-60.

Panteleyev, A., 1980, Cassiar map-area: British Columbia Ministry Energy, Mines, Petroleum Resources, Paper 1980-1, p.80-88.

Roedder, E. and Bodnar, R.J., 1980, Geologic pressure

determinations from fluid inclusion studies: Annual Review Earth Planetary Sciences, v.8, p.263-301.

Sasaki, A. and Ishihara, S., 1979, Sulfur isotopic composition of the magnetite-series and ilmenite-series granitoids in Japan: Contributions Mineralogy Petrology, v.68, p.107-115.

Sasaki, A. and Ishihara, S., 1980, Sulfur isotope characteristics of granitoids and related mineral deposits in Japan: Proceedings 5th Quadrennial I.A.G.O.D. Symposium, p.325-335.

Schuler, C. and Steiger, R.H., 1978, On the genesis of feldspar megacrysts in granites - An Rb/Sr isotopic study: United States Geological Survey, Open File Report, 78-701, p.386-387.

Shimazaki, H. and Yamamoto, M., 1979, Sulfur isotope ratios of some Japanese skarn deposits: Geochemical Journal, v.13, p.261-268.

Steiger, R.H., and Jager, E., 1977, Subcommission on geochronology: convention on the use of decay constants in geo- and cosmochronology. Earth Planetary Science Letters, v.36, p. 359-362.

Strecheisen, A., 1974, Classification and nomenclature of plutonic rocks: Geologische Rundschau, v.63, p.773-786.

Strong, D.F., 1981, Ore deposit Models - 5. A model for granophile mineral deposits: Geoscience Canada, v.8, n.4, p.155-161.

Tanaka, K., and Nozawa, T., 1977, Geology and Mineral Resources of Japan, Volume 1 - Geology, Geological Survey Japan.

Taylor, B.E. and O'Neil, J.R., 1977, Stable isotope studies of metasomatic Ca-Fe-Al-Si skarns and associated metamorphic and igneous rocks, Osgood Mountains, Nevada: Contributions Mineralogy Petrology, v.63, p.1-49.

Tempelman-Kluit, D.J., 1979, Transported cataclasite, ophiolite and granodiorite in Yukon - Evidence of arc-continent collision: Geological Survey Canada, Paper 79-14, 27p.

Tischendorf, G., 1977, Geochemical and petrographic characteristics of silicic magmatic rocks associated with rare element mineralization: Metallization associated with acid magmatism, ed. M. Stemprok, v.3, p.41-96.

Wanless,R.K., Loveridge, W.D. and Mursky, G., 1968, A geochronological study of the White Creek batholith, southeastern British Columbia: Canadian Journal Earth Science, v.5, p.375-386.

White, A.J.R. and Chappell, B.W., 1977, Ultrametamorphism and

granitoid genesis: Tectonophysics, v.43, p.7-22.

White, A.J.R., Williams, I.S. and Chappell, B.W., 1977, Geology of the Berridale: New South Wales Geological Survey, 1:100,000 sheet 8625, p.1-138.